LUND UNIVERSITY

The Co-Structure Directing Agent (CSDA) Approach to Mesoporous Silica Formation – Exploring the Assembly Characteristics

Lin, Ruiyu

2016

Document Version:
Publisher's PDF, also known as Version of record

Link to publication

Citation for published version (APA):
Lin, R. (2016). *The Co-Structure Directing Agent (CSDA) Approach to Mesoporous Silica Formation – Exploring the Assembly Characteristics*. Lund University, Faculty of Science, Department of Chemistry, Division of Physical Chemistry.

Total number of authors:
1

General rights
Unless other specific re-use rights are stated the following general rights apply:
Copyright and moral rights for the publications made accessible in the public portal are retained by the authors and/or other copyright owners and it is a condition of accessing publications that users recognise and abide by the legal requirements associated with these rights.
• Users may download and print one copy of any publication from the public portal for the purpose of private study or research.
• You may not further distribute the material or use it for any profit-making activity or commercial gain
• You may freely distribute the URL identifying the publication in the public portal

Read more about Creative commons licenses: https://creativecommons.org/licenses/

Take down policy
If you believe that this document breaches copyright please contact us providing details, and we will remove access to the work immediately and investigate your claim.

LUND UNIVERSITY

PO Box 117
221 00 Lund
+46 46-222 00 00

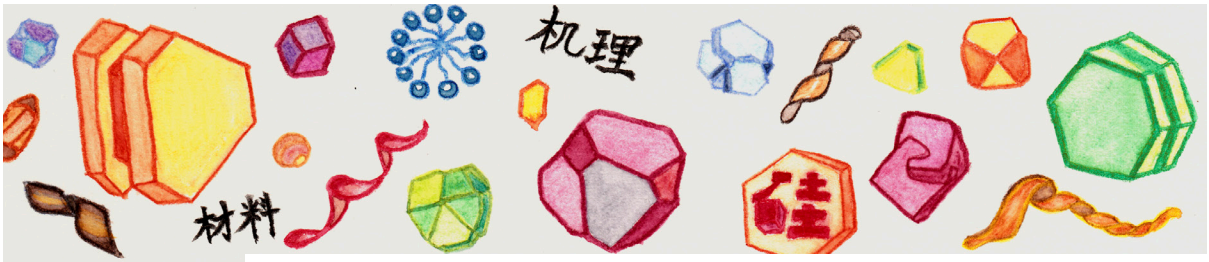

The Co-Structure Directing Agent (CSDA) Approach to Mesoporous Silica Formation - Exploring the Assembly Characteristics

RUIYU LIN | PHYSICAL CHEMISTRY | FACULTY OF SCIENCE | LUND UNIVERSITY

The Co-Structure Directing Agent (CSDA) Approach to Mesoporous Silica Formation

– Exploring the Assembly Characteristics

Ruiyu Lin

LUND
UNIVERSITY

DOCTORAL DISSERTATION
by due permission of the Faculty of science, Lund University, Sweden.
To be defended on 25 November 2016, at 13:15 in lecture hall B,
Centre for Chemistry and Chemical Engineering, Lund.

Faculty opponent
Mika Lindén
Institute of Inorganic Chemistry II,
Ulm University, Ulm, Germany

Organization
LUND UNIVERSITY

Division of Physical Chemistry
P.O. Box 124
221 00 Lund, Sweden

Author(s)
Ruiyu Lin

Document name
DOCTORAL DISSERTATION

Date of issue
2016-11-01

Sponsoring organization

Title and subtitle
The Co-Structure Directing Agent (CSDA) Approach to Mesoporous Silica Formation – Exploring the Assembly Characteristics

Abstract
We investigate the formation mechanism responsible for two specific systems of mesoporous silicas formed with the so-called co-structure directing agent (CSDA) route. The synthesis relies on the interactions between silica source (tetraethylorthosilicate, TEOS), surfactants and CSDA. The structures of the mesoporous silica materials were investigated mainly by small angle X-ray diffraction (SAXD), supplemented with transmission electronic microscopy (TEM). The surfactant/water system was investigated mainly by small X-ray scattering (SAXS).

In system 1, a cationic surfactant ($C_{18}H_{37}N^+(CH_3)_2(CH_2)_3N^+(CH_3)_3Br_2$) and an anionic CSDA (carboxyethylsilanetriol, CES) are used. We have insight into the surfactant aqueous solution, the formation kinetics (reactions of TEOS), and the electrostatic interactions (addition of salt or controlling the concentration of CSDA). Depending on the concentration of HCl in the synthesis, the structure is defined by $Fm\bar{3}m$ (at high pH) and by $Fd\bar{3}m$ (at low pH), with a gradual transition in the intermediate pH range. When salt is added in the $Fd\bar{3}m$ synthesis, the $Pm\bar{3}n$ structure is formed. The micellar sizes of $C_{18\text{-}3\text{-}1}$ assembled in these three structures are the same. Using SAXD and ^{13}C PT ssNMR, we followed the synthesis process of these three structures, and found that a fast process results in $Fm\bar{3}m$, regardless of pH, and a slow process results in $Fd\bar{3}m$. When NaCl is added to the slow system (low pH) the formation is altered resulting in a material with the $Pm\bar{3}n$ structure. We suggest that the materials strive to form the densest structure possible which structure that forms depends on the when the condensation of the silica network arrests the formation process. We also investigate the difference of this system with that of a reversed system (i.e. based on an anionic surfactant and a cationic CSDA). We find both similarities and differences between these two “mirroring” systems.

In system 2, an anionic surfactant (*N*-myristoyl-L-alanine, C_{14}-L-Ala) and cationic CSDA (3-aminopropyltriethoxysilane, APES) are used. The cryo-TEM and cryo-SEM images provide detailed information about the formation process of the material. A formation mechanism is suggested. The fibers grow in width. The ribbons twist, and with time grow in width, eventually forming helical ribbons. Later on the helical ribbons merge into tubes. This evolutionary progress of the configuration could be explained by the incompatible elastic sheet theory.

Key words
mesoporous silica materials, co-structure directing agent, surfactants, mesostructures, scattering, NMR, TEM

Classification system and/or index terms (if any)

Supplementary bibliographical information

Language
English

ISSN and key title

ISBN
978-91-7422-483-2 (print)
978-91-7422-484-9 (pdf)

Recipient’s notes

Number of pages
192

Price

Security classification

I, the undersigned, being the copyright owner of the abstract of the above-mentioned dissertation, hereby grant to all reference sources permission to publish and disseminate the abstract of the above-mentioned dissertation.

Signature  Date 2016-10-21

The Co-Structure Directing Agent (CSDA) Approach to Mesoporous Silica Formation

– Exploring the Assembly Characteristics

Ruiyu Lin

LUND
UNIVERSITY

Cover image designed by Ruiyu Lin, with help from Mireille Mooij,
Mirelle Art Production, Sweden.

Profile on the back cover designed by Yanche Chen,
Keys Art, China.

Copyright © Ruiyu Lin, 2016

Division of Physical Chemistry
Department of Chemistry
Lund University

ISBN 978-91-7422-483-2 (print)
ISBN 978-91-7422-484-9 (pdf)

Printed in Sweden by Media-Tryck, Lund University
Lund 2016

Contents

List of Papers

This thesis is based on the work presented in the following papers. The papers are appended at the end of the thesis and referred to by their Roman numerals.

I **Two Micellar Structures, $P6_3/mmc$ and $Pm\bar{3}n$, in a Divalent Cationic Surfactant/water System – Characterization and Structure Relationship**
Ruiyu Lin, Carola J. Müller, Ulf Olsson, Viveka Alfredsson and Olle Söderman
Submitted

II **Kinetic Influence of Siliceous Reactions on Structure Formation of Mesoporous Silica Formed via the Co-Structure Directing Agent Route**
Ruiyu Lin, Göran Carlström, Quoc Dat Pham, Michael W. Anderson, Daniel Topgaard, Karen J. Edler, and Viveka Alfredsson
J. Phys. Chem. C, **2016**, 120 (7), 3814–3821

III **Influence of Salt on the Formation of Mesoporous Silica Formed via the Co-Structure Directing Route**
Ruiyu Lin, Göran Carlström, Daniel Topgaard, Ulf Olsson, Karen J. Edler, Shunai Che and Viveka Alfredsson
Submitted

IV **Structure Diagram Comparision of Two Opposite Mesoporous Silica Synthesis Systems: Cationic Surfactant and Anionic CSDA vs. Anionic Surfactant and Cationic CSDA**
Ruiyu Lin and Viveka Alfredsson
Manuscript

V **A cryo-EM Study of the Formation of Helical Ribbons of Mesoporous Silica Materials**
Ruiyu Lin, Mingming Zhang, Yeshayahu (Ishi) Talmon and Viveka Alfredsson
Manuscript

List of Contributions

Paper I. I designed and performed all the experimental work. I made all analysis with help from the co-authors. I wrote the manuscript with input from the co-authors.

Paper II. I participated in designing the study. I performed all experiments, and analyzed the data with help from the co-authors. I wrote the manuscript with input from the co-authors.

Paper III. I participated in designing the study. I performed all experiments, and analyzed the data with help from the co-authors. I wrote the manuscript with input from the co-authors.

Paper IV. I designed and performed all the experimental work, some with help from co-workers. I wrote the manuscript with input from the co-author.

Paper V. I participated in designing the study. I performed all experiments, but the TEM measurements were done by co-authors. I analyzed the data. I was responsible for writing the manuscript.

List of Abbreviations

^{13}C PT ssNMR	^{13}C Polarization Transfer solid-state NMR
2D	two-dimensional
AMS	anionic surfactant templated mesoporous silica
APES	3-aminopropyltriethoxysilane
APS	3-aminopropyltrimethoxylsilane
C_{14}-L-Ala	*N*-myristoyl-L-alanine
$C_{18\text{-}3\text{-}1}$	octadecylpentamethyl-1,3-propylenebis (ammonium bromide)
CCP	cubic close packed
CES	carboxyethylsilanetriol sodium salt
Cryo-TEM	Cryogenic Transmission Electron Microscopy
CSDA	co-structure directing agent
CTAB	cetyltrimethyl-ammnonium bromide
DLS	dynamic light scattering
DTAC	dodecyltrimethylammonium chloride
HCP	hexagonal close packed
IUPAC	International Union of Pure and Applied Chemistry
MSMs	mesoporous silica materials
NMR	Nuclear Magnetic Resonance
PDDF	pair-distance distribution function
PEO	polyethylene oxide
PPO	polypropylene oxide
SAXD	Small Angle X-ray Diffraction
SAXS	Small Angle X-ray Scattering
SBA	Santa Barbara Amorphous
SEM	Scanning Electron Microscopy
TEM	Transmission Electron Microscopy
TEOS	tetraethyl orthosilicate
TMAPS	*N*-trimethoxysilylpropyl-*N,N,N*-trimethylammonium chloride

Popular Science Summary

This thesis is focused on the detail process of formation of mesoporous silica materials.

Mesoporous silica materials are one type of porous materials with a pore size between 2 and 5 nm (1 nm=0.000 000 001 m). The pore walls consist of silicon dioxide – silica (sand also consists of silica). The mesoporous silica materials are formed by amphiphilic molecules, a kind of molecule with one part that loves water and one part that hates water, and a silica source. Within the group of amphiphilic molecules, surfactants are mostly used. Surfactants are molecules that can have positively or negatively charged head groups, which attract water, and long organic tails, that repel water. Examples of surfactants in our daily life are shampoos and detergents. When surfactants are dissolved in water, the organic tails will cluster together and only leave the charged head groups outside in contact with the water. In this case, the aggregated surfactants can form different shapes with the tails inside and the head groups on the surface of the aggregate. The silica components will decorate these aggregates and give rise to an attraction that draws the aggregates together. Accordingly, the "mesopores" of the materials are filled with surfactants during their creation. When the surfactants are removed, the mesopores arise, and the mesoporous materials with silica walls are formed. The networks of mesopores are often well ordered in various structures. When we add acid or salt into the formation mixture of mesoporous silica materials, the structure of the materials can sometimes be changed. The process is like baking, where by adding different ingredients, such as baking powder or salt, the shape or texture of the pastries can be changed.

In the work of this thesis, two recipes were used. We call them two synthesis systems. Both systems contain a molecule that eventually gives rise to the creation of the silica wall. We call this molecule the silica source. In system 1, a surfactant with a large positively charged head group was used, while in system 2, a surfactant with a negatively charged head group was used. Moreover, a molecule consisting of a charged part and a silica part was added in the mixture. In this thesis, the latter type of molecule is called CSDA. In system 1, the charged part of the CSDA is negative, and is called the carboxylate group, in vinegar there is a lot of carboxylic groups. In system 2, the charged

part is positive, with the chemical name quaternary ammonium group, which is a common component used in softeners. In the mixture, the CSDA will be in contact with the surfactant head group *via* the charged part and with the silica source *via* the silica part. After the formation, when the surfactants are removed, the charged groups of the CSDA will remain within the pores, therefore, the materials are functionalized with the charged groups of the CSDA directly in the synthesis.

In system 1, addition of acid can change the structures of the materials. In this work we aim to find reasons for the structural change. We found that addition of acid will change the building-up of the silica source. With low acid addition, the silica sources build up walls around the surfactant head groups very fast, whereas with a higher amount of acid, the silica walls build slower. If salt is added in the slower system, a different structure will be formed. This is because the added salt makes the building work even slower.

In system 2, we used a special type of instrument, called cryo-EM, to look at the system. This instrument allows us to visualize very small things (hundreds of nm in size) in frozen samples. So we can freeze samples after different formation times, and check what has been built up at these specific times. We found that in this system, the material first forms fibers, and then the fibers grow in width and form ribbons. The ribbons then twist and, with time, grow in width to eventually become helical ribbons that later merge into tubes. We also found that a mathematical model can be used to explain this shapechange process.

Acknowledgments

I spent four years doing my PhD in Sweden. These years have marked a great period of my life. I am grateful for everyone who provided me help and shared company with me in a way or another.

First of all, I would like to thank my dearest supervisor, Viveka Alfredsson. Your patience, positive comments and nice discussions mean a lot to me. You encourage me to have open conversations. I was moved a lot by so much effort you have put helping me. It is my fortune and honor to have a supervisor nice as you. You are the best supervisor in the world!

My sincere thanks also goes to my co-supervisors, Lennart Piculell, for the inspiring discussions and for proof reading my thesis, and my Chinese supervisor, Shunai Che, for introducing me to Viveka, for the helpful discussions and for providing the chemicals for my thesis work. I really appreciate all your help.

Besides my supervisors, I thank our coauthors, Ulf Olsson, Olle Söderman, Carola J. Müller, Karen J. Edler, Daniel Topgaard, Göran Carlström, Quoc Dat Pham, Michael W. Anderson, Mingming Zhang, Yeshayahu (Ishi) Talmon. Thank you for the nice cooperation and for the effort on our papers.

I would like to thank Emelie, both my colleague and my best Swedish friend, for knowing everything, helping me, taking care of me, and sharing opinions with me. Sofi, I enjoyed sharing my entire PhD life together with you. Thank you for the nice company. I also thank my other group mates and office mates, past and present, Julien, Yana, Tomas, Ricardo, Jenny, Jon… Thank you for your kind help in research and in life.

I thank Gunnel for the TEM and cryo-TEM images, Maria V. for TEM profiles, Marta, Thiago and Luigi for the informative conversations about scattering. Lu Han, Yanhang Ma and Zhehao Huang, thank you for the long distance discussions and your kind help about the structures.

Thanks to Ingrid Nilsson, Helena Persson, Maria Södergren and Christopher Hirst, without you, nothing would ever happen at our division.

I would especially thank Saskia, Solmaz, Johanna, Divya and Emelie (again). We shared a lot of wonderful moments during these years. You are like sisters to me. Thank you for taking care of me so well.

Dat, thank you for doing NMR experiments for me during the weekends, for helping with my thesis, and for sharing plenty of opinions, interests and moods. You are such a sweet friend to me.

Our present lunch group, Antara, Jin and Julien, thank you for the tasty food and enjoyable chats. You helped me to survive during my thesis working period.

A big thanks goes to all of my current and former colleagues from the division of Physical Chemistry and Theoretical Chemistry, for the friendly atmosphere, interesting discussions and fascinating events. Because of you, my PhD life is much happier than I could imagine. Special thanks also to my Chinese colleagues, Xiaoting, Hongduo, Feifei, Fei, Weimin and Meina. You are amazing friends. Thank you for everything!

To all my Chinese friends both in Sweden and in China, thank you for your kind care and encouragement. Especially to Mona, thank you for sharing good deep thinking about our PhD life. I feel lucky to be your friend since we met in Sweden and I still do. I cherish our friendship very much. Kena and Hong J., it was so nice of you to cook for me during my busiest time. Your food made me happy and made me work energetically.

To my family,

My dear husband Jian, thank you for understanding me and for taking care of me all the time. You are so wise, so responsible, and so cute. I love you so much! If any person does not trust marriage, I would think that is because they have not met someone like you.

My dear parents, you are the ones I want to thank the most. You are always there, trust me, care about me and share my happiness and complaints. Although I'm far away from home now, my heart is always close to you. I would also like to thank my in-laws for their support.

亲爱的爸爸妈妈，我爱你们！

Ruiyu Lin (Jessie)

林芮羽

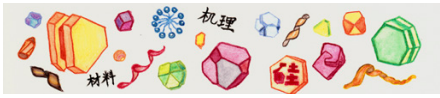

Introduction

1 Introduction

Porous materials are frequently used in our daily life, for example, the sponge we use for cleaning the dishes and the filter paper to make coffee. We get benefits from their porous network for separation and from their large total surface area for adsorption. The study of porous materials has been an interesting field for a long time because the materials can be used in many applications. On the other hand, considering the numerous porous materials in nature, for instance honeycomb, wood, and bone, the studies of porous materials are also very helpful for us to understand how materials in nature function.

If the porous material has an organized porous network and a porous diameter sufficiently small to form a so-called nanoporous material, it can be used for applications directed at molecular scale processes due to its large surface area and pore volume. These applications include catalysis, drug delivery, and energy storage. Because of the promising perspective of all these applications, the research and design of nanoporous materials are becoming more and more interesting and important.

Nanoporous materials consist of a regular organic or inorganic framework that generates a porous structure. According to the definition by IUPAC (the International Union of Pure and Applied Chemistry),[1] nanoporous materials are classified by the size of their pores: microporous (less than 2 nm), mesoporous (2–50 nm) and macroporous (larger than 50 nm). In the family of nanoporous materials, the silica materials are the largest group. They are also the ones that are most amenable for design and synthesis. Well-known examples of silica-based porous materials are zeolites that are microporous, opals that are macroporous and mesoporous silicas.

Zeolites are crystalline aluminosilicates, which consist of a framework built up by Si (or Al) tetrahedrally coordinated to O, with uniform pore sizes less than 2 nm.[2] Zeolites occur naturally and are also produced industrially on a large scale with higher purity and more diverse structures than the ones found in nature.[3] They are commonly used as commercial adsorbents and in catalysis and are also an important constituent in washing powder where they function as ion-exchangers.[4] Moreover, since zeolites have uniform pore size, they have the ability to selectively sort molecules. Hence, zeolites are also

known as “molecular sieves”. However, limited by the restricted pore size, zeolitic molecular sieves can only be applied for small molecules.

Opal is a hydrated amorphous form of silica, which is different from the crystalline forms of silica. It occurs in fissures of rock, and is known as precious opal. Opals are composed of silica spheres with sizes from 150 to 300 nm in diameter.[5-6] Opals can also be synthesized, however with lower density.[7-8] Although macroporous materials have a larger pore size, they also generally have a wide pore size distribution. Therefore they have limited use in adsorption and separation applications. The macroporous opaline materials are usually used in the photonic fields.[8-9]

Mesoporous silica materials are, as mentioned above, materials having an interconnected network of pores with pore sizes between 2 and 50 nm. They are typically ordered but mesoporous materials with disordered pore systems also exist, for instance aerogels or pillared clays.[10] They not only have the pore size region between zeolites and macroporous opal, but also have characteristics in between these two types of materials; the pores have long-range-ordering while the framework is amorphous. Mesoporous silica materials are considered “cavity crystals” and are synthetic materials. The typical method of synthesis is to use amphiphiles as templates and let silica oligomers aggregate around the amphiphilic aggregates. This process eventually leads to the formation of an inorganic/organic composite material that has a mesostructure. Thanks to the various amphiphiles, mesoporous silica materials can be synthesized with diverse structures. Because of the highly ordered mesostructures, good surface properties, and appropriate pore size, applications of mesoporous silica materials range from use as drug carrier, to catalysis and to separation for large molecules. However, the amorphous silica framework of mesoporous materials is typically not as strong as the crystalline framework of, for instance, zeolites, which makes the materials more vulnerable to experimental conditions, such as high temperatures. This is a limitation for the use of mesoporous silica materials in catalysis, where re/use of the material is an essential factor.

It is important to understand the formation mechanism of the materials because it can allow us to rationally design new materials to meet the specific demands of the broad range of applications, to develop environmentally friendly materials and synthesis methods, and it can provide insight into the formation procedures of the analogous materials in nature. The aim of this thesis is to expand the understanding of the formation mechanism of the syntheses of mesoporous silica materials. Two specific systems are selected in this study, both being based on the so-called co-structure directing agent approach, which is explained in more detail in Chapter 3.

This book is divided into sections, starting with the introduction part including background (Chapter 2 and 3) and experimental techniques (Chapter 4), followed by the results part where the key results are summarized (Chapter 5 and 6) and finally the conclusion and future perspectives are stated (Chapter 7). The scientific papers are

included at the end of this thesis. Two synthesis systems are considered in this work; the main part of the thesis, paper I to paper IV, are related to system 1, and paper V is related to system 2.

2 Mesoporous Silica Materials

Mesoporous materials were first developed more than 20 years ago. In the early 1990s, mesoporous silica materials (MSMs) were synthesized by two groups: Kuroda's group at Waseda University, Japan, and Kresge's group at the Mobil Company, USA.[11-13] The MSMs synthesized by Mobil's researchers are named the M41S series,[12-16] which includes three types of structures, MCM-41 with a two-dimensional (2D) hexagonal structure,[14] MCM-48 with a bicontinuous cubic porous network,[15] and MCM-50 with a layered structure. Later on, with the developments of new synthesis systems, a lot of new structures of mesoporous materials with different characteristics were discovered. There were other families of mesoporous silicas appearing, for example the SBA series[17-22] and the AMS series.[23]

So far, just after two decades, scientists have developed a large number of mesoporous materials with different compositions, structures, morphologies and functions. The study of the formation mechanism of mesoporous materials has become more and more important in order to find ways to rationally design materials and to meet the demands for the varying types of applications, such as catalysis, chemical separation, hard template, functional adsorption, and drug delivery.

This chapter gives a brief introduction to the synthetic route, the proposed formation mechanism, and the mesostructure control of MSMs.

2.1 Synthesis of mesoporous silicas

The typical synthesis strategy of MSMs is to use amphiphiles as structure-directing agents in an aqueous solution. The formation is based on the amphiphile self-assembly. Polymerization of a silica source builds up the walls around and in between the amphiphilic aggregates. The driving force for formation relies on an attractive interaction between the hydrophilic part of the amphiphile and the inorganic silica source.[24] During the synthesis step the material forms the structure. After completion of the synthesis step,

and under hydrothermal condition, the silica is further condensed. Removal of the amphiphiles after completed synthesis establishes the porous network.

Overall, the syntheses can be designed by using different amphiphiles and controlling the reaction conditions, such as temperature, pressure and solution conditions. For example, in the M41S series of materials, a cationic surfactant is used as a template and the syntheses are performed under strongly basic conditions,[12-13] whereas in the SBA series of materials, the syntheses are mostly performed under strong acidic conditions. For the SBA family, SBA-1, 2 and 3 are based on cationic surfactants templating,[19-20] SBA-11, 12 and 14 are synthesized using nonionic surfactants and SBA-15 and 16 are made using triblock copolymers, such as polyethylene oxide-polypropylene oxide-polyethylene oxide (PEO-PPO-PEO), as the structure-directing agent.[21-22] In the AMS series, anionic surfactants and an additional synthesis component, a so-called co-structure directing agent, are used in the synthesis. This latter synthesis strategy is described further and in more detail in Chapter 3.

The mechanisms of the syntheses of MSMs generally rely on two chemical processes working hand in hand: self-assembly of the structure directing agent and the reactions of the silica source, i.e. hydrolysis and condensation reactions.[25] The synthesis mainly involves four types of substances: the inorganic species, the template, the solvent, and the ions in the solution. The inorganic species is the silica source. The most popularly used silica sources are alkoxysilanes. In this thesis work, tetraethyl orthosilicate (TEOS) is used. As explained above, the amphiphilic molecules act as structure directing agents, or templates. They can be classified as surfactants or amphiphilic block copolymers. Here, mainly surfactants are discussed. The most frequently used solvent is water, but a less polar solvent like alcohol can also be used.[26] The ions in the solution are the surfactant counterions, ions from the base or acid added, or additional ions from added salts. Both the identities and the concentrations of the various ions play an important role in the synthesis. Both the identities and the concentrations of the various ions play an important role in the synthesis.[17, 24] Among these four substances, the structure directing agent (surfactant) and the silica source are believed to have key roles in the formation of MSMs. However, the detailed interactions between the components has yet to be clarified.

Next, the properties of surfactants and the silica chemistry is introduced.

2.1.1 Structure directing agent – Surfactants

Molecules that are widely used as templates in the synthesis of MSMs are amphiphilic surface-active agents, surfactants, which consist of at least two parts, a water-soluble hydrophilic head group and a water-insoluble hydrophobic tail. Surfactants can be grouped into two types, ionic surfactants and nonionic surfactants. Ionic surfactants are:

cationic, with positively charged head groups, such as CTAB; anionic, with negatively charged head groups, such as carboxylate and sulfate head groups; or zwitterionic surfactants, containing both cationic and anionic centers. The nonionic surfactants are mostly alkyl polyethylene oxides, where the alkyl chain (C_n, containing n carbons) is the hydrophobic part and the chain of ethylene oxide (EO_m, containing m EO groups) is the hydrophilic part.

When surfactants dissolve in water, they will adsorb at the water-air interface or at the interface between water and other hydrophobic compounds. The hydrophobic tail of the surfactant will extend out of the bulk water phase, towards air or towards a hydrophobic component, while the hydrophilic head group remains in the water phase. In the bulk aqueous phase, when surfactants exceed the critical micelle concentration (CMC), they aggregate to form micelles, where the hydrophobic tails form the core of the micelle and the hydrophilic heads are in contact with the surrounding liquids, forming a corona. Besides the surfactants' own characteristics, the CMC can be influenced for instance by addition of salt or by temperature.

In a concentrated surfactant aqueous solution, typically well above CMC, the surfactant self-assembles into liquid crystalline phases. The structure of the liquid crystalline phase depends on the packing of the surfactant molecules into the micelles. The packing parameter of the molecules relies on their effective head group area (a_0), the volume (v) of their hydrocarbon chain and the length of their hydrocarbon chain (l_c), which gives the dimensionless number, $v/a_0 l_c$ – the packing parameter. When $v/a_0 l_c$ increases, the surfactant has a propensity to form structures, from spherical micelles ($v/a_0 l_c \leq 1/3$) to non-spherical or ellipsoidal micelles ($1/3 < v/a_0 l_c < 1/2$) to cylindrical or rod-like micelles ($v/a_0 l_c \approx 1/2$) to bicontinuous structures ($1/2 < v/a_0 l_c < 1$) to vesicles and bilayers ($v/a_0 l_c \approx 1$) with a lamellar structure, and finally to a group of "inverted" micelles ($v/a_0 l_c > 1$).[27] This transformation is illustrated in Figure 2.1.

The packing parameter varies not only with the shape of the surfactant molecule but is also sensitive to the conditions of the solutions as mentioned above. For example, addition of salt is expected to have an influence on structures formed in ionic surfactant water solutions.[28] The additional counterions screen the repulsion between the head groups leading to a decrease in the head group area. With the length and volume of the surfactant tail unchanged, the surfactant packing parameter will hence increase, favoring structures with lower curvature. This typically results in an increase of the surfactant aggregation number and a decrease of CMC.[28]

In a simple surfactant/water system, the self-assembly usually begins with spherical micelles, randomly distributed in an isotropic dilute solution. As the surfactant concentration increases, the micelles first organize into a micellar cubic phase, then the aggregate shape changes resulting in hexagonal, bicontinuous cubic and lamellar structures (Figure 2.1). A typical well-known example is the phase behavior of DTAC.[29]

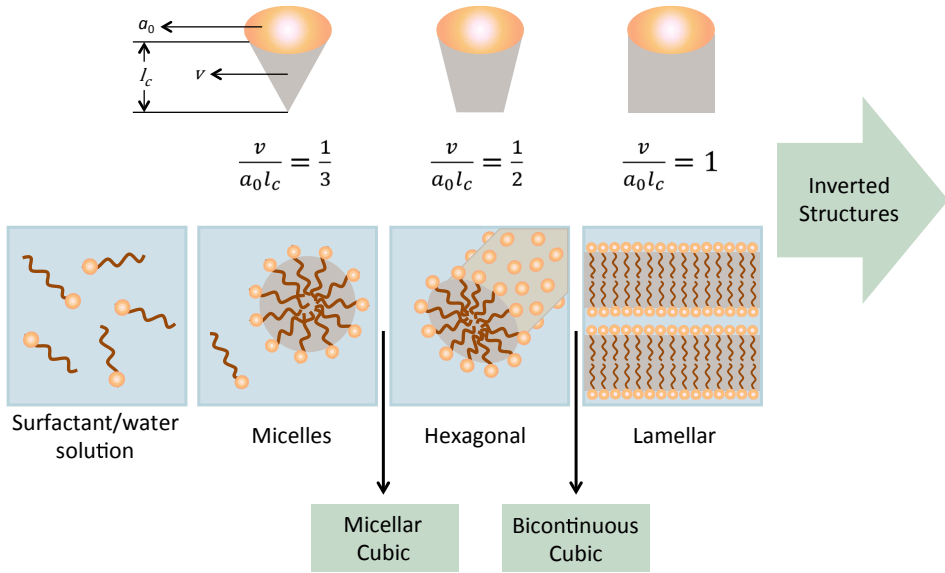

Figure 2.1. Critical packing parameters of surfactant molecules and preferred aggregate structures for geometrical packing reasons and "mesophases" formed by surfactants in aqueous solutions.

Compared to the surfactant/water liquid crystal system, ordered mesoporous silica has a skeletal wall made up of amorphous silica instead of water. The surfactants act as the structure directing agent during the synthesis and silica condenses in the vicinity of the head groups. The "mesopores" are filled with surfactants during synthesis. It is only after removal of the surfactant that the porous structure arises.

2.1.2 Reaction of silica

The synthesis of MSMs is based on the following reactions of siliceous species. For the alkoxysilanes that are normally used as a silica source, the reactions are based on hydrolysis and polymerization (or condensation). In solution, the alkoxysilanes are hydrolyzed and condensed to form polymeric species composed of Si-O-Si bonds. Generally, three reactions can be used to describe the process: hydrolysis (eq. 2.1), alcohol condensation (eq. 2.2) and water condensation (eq. 2.3).

$$\equiv Si{-}OR + H_2O \rightleftharpoons \equiv Si{-}OH + ROH \quad (2.1)$$

$$\equiv Si - OR + HO - Si \equiv \rightleftharpoons \equiv Si - O - Si \equiv + ROH \quad (2.2)$$

$$\equiv Si - OH + HO - Si \equiv \rightleftharpoons \equiv Si - O - Si \equiv + H_2O \quad (2.3)$$

At the beginning of the reaction, the silica source hydrolyzes and then polymerizes to water-soluble silicate oligomers, then, the polysilicates further condense and form three-dimensional networks. The hydrolysis occurs by nucleophilic attack of the oxygen contained in water on the silicon atom;[30] and the polymerization to form siloxane bonds occurs by either an alcohol-producing condensation reaction (eq. 2.2) or a water-producing condensation reaction (eq. 2.3).[31] Knowledge of the mechanisms and kinetics of these reactions provides insight into the structural formation of the mesoporous silica materials.

The hydrolysis and polymerization rates are highly dependent on pH. Figure 2.2 shows a schematic representation of the pH dependencies of the hydrolysis, condensation, and depolymerization rates as summarized by Brinker in 1988.[30] According to Figure 2.2, if we use TEOS as an example, the hydrolysis rate of TEOS reaches a minimum at a pH around 7. The condensation on the other hand shows a reverse behavior with the highest rate just around pH 8.[30, 32] Hence, control of pH plays a significant role in the reaction rates of silica and is an important parameter in the synthesis of MSMs.

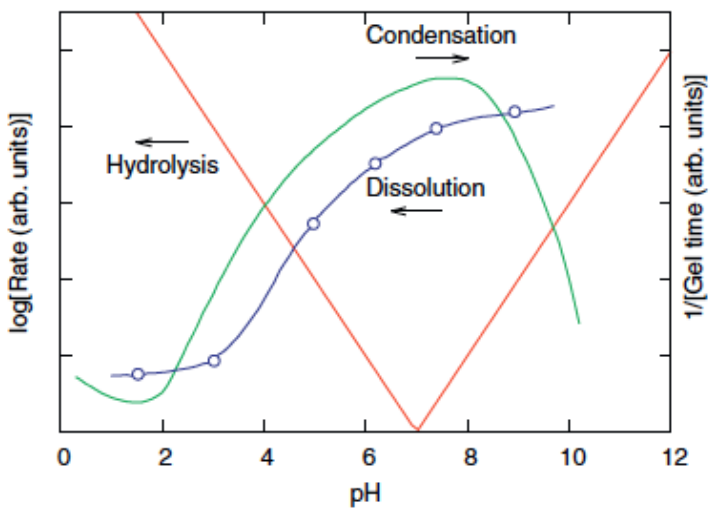

Figure 2.2. Schematic representation of the pH dependences of the hydrolysis, condensation, and dissolution rates. After Refs. 30, 32.*

*Reprinted from Journal of Asian Ceramic Societies, Vol. 1, Koichi Kajihara, Recent advances in sol–gel synthesis of monolithic silica and silica-based glasses, Page 125, Open Access funded by Ceramic Society of Japan and Korean Ceramic Society Under a Creative Commons license. The original figure is from Journal of Non-Crystalline Solids, Vol. 100, C.J. Brinker, Hydrolysis and condensation of silicates: Effects on structure, Pages 47, Copyright (1988), with permission from Elsevier.

Besides pH, the reaction of silica also depends strongly on the temperature, the concentration of the inorganic species, and the reaction time. Addition of salt also has an influence. For example, a solution of silicates can precipitate in the presence of NaCl. The precipitate is readily re-dissolved if the system is diluted with water.[31]

As explained above, the syntheses of mesoporous silica materials are related to the structure promoter (surfactant) and the inorganic species (silica). But more knowledge is needed in order to understand the mechanism of the entire synthesis process, for example the self-assembly of surfactants under the synthesis conditions, the kinetics of the silica reactions, the interactions between surfactants and silica, and their mutual temporal evolution (the dynamics).

Many different mechanisms have been suggested in previous studies. They all provided the knowledge only to explain certain specific systems. However, no general understanding of the accurate synthesis process has been discovered for MSMs. In the other words, more specific investigations are needed.

2.2 Meso-structure types

A simple inorganic crystal has a structure with a repeated lattice of atoms or molecules, but liquid crystal structures and mesoporous materials have a repeated packing of micelles and ordered pores. The order is on a different length scale than in a simple inorganic crystal; it is structured on the mesoscale, and hence we call it mesostructure. There are different types of mesostructures: micellar cubic, 2D columnar, bicontinues, and lamellar structures.

Like the simple inorganic crystalline structures, mesostructures can be described by the lattice parameter of the unit cell and the symmetry of the ordering. Unit cells are basic building blocks of the crystals that pack together to fill space. A unit cell of a 3D lattice is a parallelepiped defined by three edge lengths a, b, and c, and three angles α, β, and γ, as shown in Figure 2.3. There are seven possible unit cell shapes that can fulfill the space filling – they are known as the seven crystal systems and their specifications are listed in Table 2.1. In addition, the 3D unit cell includes four different lattice types: the primitive unit cell (symbol P), the body-centered unit cell (symbol I), the face-centered unit cell (symbol F) that has lattice points in the center of each face, and the other face-centered unit cell (symbol A, B, or C) that has lattice points in the centers of one pair of opposite faces. When these four types of lattice are combined with the 7 possible unit cell shapes, 14 permissible Bravais lattices (Table 2.1) are produced.

The symmetry of a crystal is a point group taken from a point at the center of a perfect crystal. Each single crystal system has its own symmetry elements. The combination of rotation, inversion, mirror and rotation inversion gives 32 crystallographic point groups.

By the combination of the 32 crystal point groups and the 14 Bravais lattices, 230 different space-filling patterns exist that crystal structures can adopt. They are the 230 space groups, which are all collected in the International Tables for Crystallography.[33]

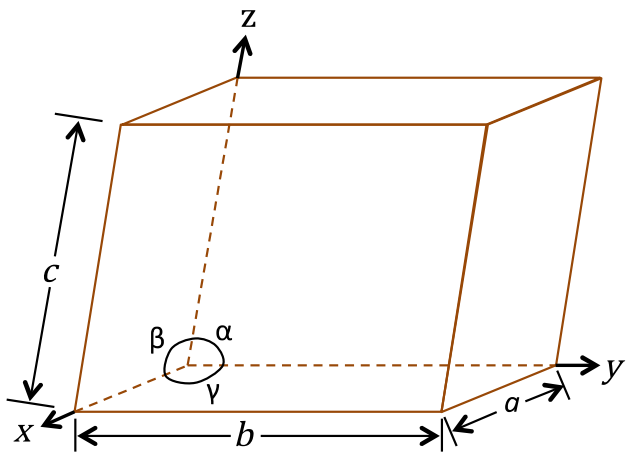

Figure 2.3. Definition of axes, dimensions and angles for a general unit cell.

Table 2.1. Bravais lattices

Crystal systems	Unit cell	Lattice types
Cubic	$\alpha = \beta = \gamma = 90^{\circ}$ $a = b = c$	P, I, F
Tetragonal	$\alpha = \beta = \gamma = 90^{\circ}$ $a = b \neq c$	P, I
Hexagonal	$\alpha = \beta = 90^{\circ}, \gamma = 120^{\circ}$ $a = b \neq c$	P
Trigonal/rhombohedral	$\alpha = \beta = \gamma \neq 90^{\circ}$ $a = b = c$	P/R*
Orthorhombic	$\alpha = \beta = \gamma = 90^{\circ}$ $a \neq b \neq c$	P, C, I, F
Monoclinic	$\alpha = \gamma = 90^{\circ}, \beta \neq 90^{\circ}$ $a \neq b \neq c$	P, C
Triclinic	$\alpha \neq \beta \neq \gamma \neq 90^{\circ}$ $a \neq b \neq c$	P

* The primitive description of the rhombohedral lattice is normally given the symbol R.

2.2.1 Micellar cubic structures

In the surfactant/water liquid crystal system, the micellar cubic phase appears at concentrations between micellar solution and hexagonal phase: the structure is typically described as 3D ordered packing of spherical micelles. In the case of MSMs with micellar cubic structures, the micelles are usually considered as spheres organized in a silica matrix. The pores are connected by small windows believed to arise from the contact area of the spherical micelles.

One of the most common micellar cubic structures is defined by the $Pm\bar{3}n$ space group, which has been observed in numerous amphiphilic systems.[29, 34-37] The $Pm\bar{3}n$ structure for the liquid crystalline phase contains 2 sites of in total 8 micelles. As summarized by Liu et al.,[38] three explanations have been proposed explaining the packing of the $Pm\bar{3}n$ structure. One suggestion is that there are two shapes of micelles in the unit cell;[39] a second one is that all the micelles have the same non-spherical, or rice-type, shapes, rotated in two different ways;[40-41] the third explanation is that the packing follows a minimal-area rule between the neighbors.[42] $Pm\bar{3}n$ is also synthesized in the MSMs, as for instance SBA-1.[20] The structure has been explained to be based on polyhedron packing, similar to the third suggestion just mentioned. The spherical micelle is considered to make an interface with the next micelles forming a polyhedron instead of perfect sphere. This packing structure is called cage-type mesoporous structure. In the cage-type MSMs, each polyhedron consists of both surfactant micelle and part of the silica wall (Figure 2.4, f). The $Pm\bar{3}n$ structure as shown in Figure 2.4 (d) is the packing of four 12-hedra (Figure 2.4, a) and six 14-hedra (Figure 2.4, b).[43]

Another cage-type mesoporous structure is the $Fd\bar{3}m$ structure, which can also be described as a stacking of two different types of polyhedra. As shown by Sakamoto and Han et al. in Figure 2.4,[43] the unit cell of the $Fd\bar{3}m$ structure (Figure 2.4, e) consists of sixteen 12-hedra (Figure 2.4, a) and eight 16-hedra (12 pentagons and 4 hexagons) (Figure 2.4, c). In amphiphilic systems, several examples of the $Fd\bar{3}m$ structure are encountered in inverted micellar phases of surfactants and lipids.[44-45] It has been described that there are 24 micelles in the unit cell of this micellar cubic phase.

In addition, there are two types of spherical close packing structures; the cubic close packed (CCP) structure, defined by the $Fm\bar{3}m$ space group, and the hexagonal close packed (HCP) structure, with the $P6_3/mmc$ space group. Figure 2.5 shows the stacking of the two lattice forms. If the spheres (spherical micelles) in the bottom layer are in position A, and the second layer is in position B, the third layer can be either in position C or A. If the progression of stacking is ABC, the structure is CCP. If the stacking is ABA, the structure is HCP.

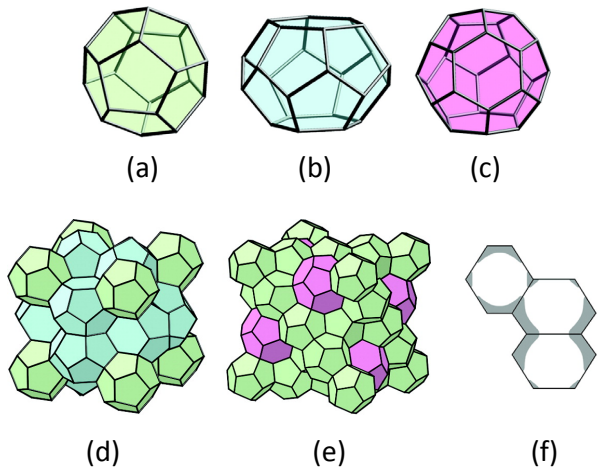

Figure 2.4. Schematic drawing of three types of polyhedra, (a) 12-hedron (5^{12}-hedron), (b) 14-hedron ($5^{12}6^2$-hedron) and (c) 16-hedron ($5^{12}6^4$-hedron); and representation of the *Pm*$\bar{3}$*n* structure (d) and the *Fd*$\bar{3}$*m* structure (e). The polyhedra occupied by micelles (white) and silica wall (gray) (f). Adapted after Ref. [43].*

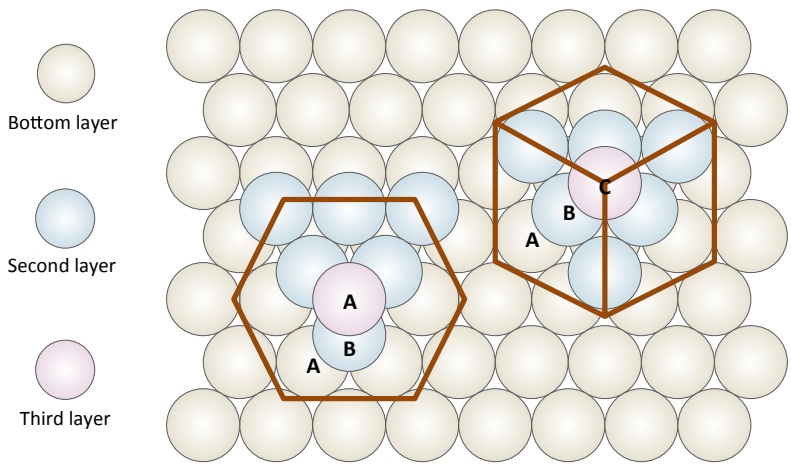

Figure 2.5. Schematic of the HCP lattice (left) and the CCP lattice (right).

* Adapted with permission from Chemistry of Materials, Vol. 21, Yasuhiro Sakamoto, Lu Han, Shunai Che, et al, Structural Analyses of Intergrowth and Stacking Fault in Cage-Type Mesoporous Crystals, Page 224, Copyright (2016), with permission from American Chemical Society.

In the case of MSMs, the interstices of the packed spherical micelles are occupied by the silica wall, and the pores are connected by small windows. Both the $Fm\bar{3}m$ structure and the $P6_3/mmc$ structure have been reported for mesoporous materials,[20, 46-47] and they have also been found as intergrowths in, for example, the SBA-12 material formed with nonionic surfactants.[22, 48]

However, in the amphiphilic/water system, the CCP and HCP structures are rarely reported. Only a few examples of the HCP structure are known. It has been observed in three types of binary systems, for a nonionic surfactant ($C_{12}EO_8$) water system,[42, 49-50] an anionic choline carboxylate surfactant-water system,[51] and recently for the cationic alkyltrimethylammonium surfactant-water system with strongly hydrated counterions.[38] The HCP structure has also been identified in other multicomponent systems, for example, for the triblock copolymer (P123) water-ethanol system,[37] in the inversed micellar lyotropic phase diagram of a mixture of different lipids in water system,[52] and in the polyion-surfactant ion complex salts in water system.[53-54] For the CCP structure, the $C_{12}EO_{12}$/water phase diagram exhibits an $Fm\bar{3}m$ phase.[55] Additionally, in the P123/water/ethanol phase diagram,[37] a mixture of CCP and HCP phases, or the only HCP phases, are observed depending on the amount of ethanol.

It has been reported that the difference of the stacking entropy of the CCP phase and the HCP phase is very weak.[56] As shown above, the experimental results confirm that these two structures are indeed related. In many reports, the CCP ($Fm\bar{3}m$) structure and the HCP ($P6_3/mmc$) structure in the phase diagram of the amphiphilic system appear between the isotropic micellar solution and the $Pm\bar{3}n$ structure phase.[50, 55]

2.2.2 2D columnar and lamellar structures

The 2D columnar mesostructure consists of rod-packing of long cylindrical micelles. The 2D hexagonal structure, with the plane group $p6mm$, is a very typical arrangement in the amphiphilic/water systems, and also very common in mesoporous silica materials, such as the well known MCM-41[14] and SBA-15.[21] In addition, there are other 2D columnar structures reported for mesoporous materials, for example, the centered rectangular structure, with the plane group $c2mm$,[57] and the 2D square structure with the plane group $p4mm$ [58].

Lamellar mesostructured mesoporous silica materials, for instance MCM-50, consist of layers of silica sheets with bilayers of amphiphiles in between. However, after removal of the surfactants, the layered structure is destroyed, and hence the lamellar structure of mesoporous materials is not as interesting as the other structures.

2.2.3 Bicontinuous structures

In the amphiphilic/water system, the bicontinuous phase occurs between the hexagonal and the lamellar phases. The term bicontinuous structure is used because it is continuous not only in the solvent but also in the surfactant arrangement. In the bicontinuous phase, the amphiphilic molecules form a porous connected structure in three dimensions. The bicontinuous cubic structures can be seen as either the connecting of rod-like micelles, similar to branched micelles, or bilayer structures. In the bicontinuous structures, the curvatures of the interface on the opposite sides are equal and with an opposite sign, leading to a small mean curvature.

In the MSMs, the bicontinuous cubic mesostructures have two disconnected but interwoven mesoporous networks divided by a silica wall. The silica wall lies on a minimal, continuously curved surface.

Three families of bicontinuous cubic structures have been discovered to date. They are the gyroid structure $Ia\bar{3}d$, the double diamond structure $Pn\bar{3}m$ and the primitive structure $Im\bar{3}m$. All of these three structures have been synthesized as MSMs. For example, MCM-48 is defined by the $Ia\bar{3}d$ structure.[15]

As introduced previously, MSMs are not just simply reproducing the structures formed by surfactants, i. e. liquid crystal structures. The structures found in mesoporous silicas not only reproduce the liquid crystals but also other structures, not previously found in liquid crystals. The synthesis not only relies on the reactants and additions present in the reaction mixtures, but is also highly dependent on the dynamics of the formation and the kinetics of the reactions.

3 The Co-Structure Directing Agent (CSDA) approach

As was introduced in Chapter 2, MSMs with different structures are generally synthesized relying on three steps/processes: the self-assembly of amphiphilic molecules that serve as structure directing agents, the chemical reactions of the silica source, and the attractive interactions between the amphiphilic aggregates and the silica species. In early works on MSMs, cationic surfactants,[11, 13] nonionic surfactants,[22] and block-copolymers[21-22] were employed as structure directing agents. The syntheses typically relied on choosing the right pH for the respective system. As an example, for cationic surfactants, the interaction between the head groups and the silica species was described as based on electrostatic interactions, and under basic conditions, the positively charged surfactant head groups interact strongly with the silica species that under those conditions are negatively charged.[17] However, anionic surfactants as structure directing molecules only resulted in lamellar and disordered mesostructures when relying on pH. This was a disappointment, as anionic surfactants are used in large volumes in industry due to their environmental friendliness and low cost; they would have been desirable in the production of MSMs. The probable reason that anionic surfactants did not work properly was suggested to be a consequence of anionic surfactants typically being weak acids or their conjugated salts, which would cause them to be protonated under acidic conditions, while under basic conditions the negatively charged surfactant head group would not be prone to bind to the negatively charged silica species. Hence no (electrostatic) attractions could be formed between the surfactant head groups and the silica source, which is necessary to form MSMs.[23, 59]

In 2003, Che and co-workers proposed a new synthesis methodology to promote interactions between the surfactants and the inorganic species, which demonstrated that anionic surfactants could also function as versatile structure promoters.[60] This method relies on introducing an additional molecule in the synthesis, an organosilane molecule that contains a charged group, typically from an acid, or a base, and a silicate group. The molecule acts as a so-called co-structure directing agent (CSDA). For syntheses that

involve anionic surfactants, the most commonly used CSDAs are 3-aminopropyltrimethoxylsilane (APS) and *N*-trimethoxysilylpropyl-*N,N,N*-trimethylammonium chloride (TMAPS). Their molecular structures are shown in Figure 3.1. In a normal synthesis, the CSDA is added together with the silica source to a surfactant aqueous solution under specific pH conditions. It has been suggested that the CSDA forms a "bridge" between the charged head group of the surfactant and the silica wall. The amino or quaternary ammonium site of the CSDA is described to interact electrostatically with the negatively charged head group of the anionic surfactant, while the alkoxysilane site co-condenses with the silica source to form a silica framework.[59] This strategy allows anionic surfactants to act as structure directors and form highly ordered MSMs; the CSDA generates the strong connection needed between silica and surfactant.

Following the CSDA route, highly ordered MSMs with various structures have been developed not only by using anionic surfactants as the template and cationic organosilane as the CSDA, but also cationic surfactants and anionic organosilane. Carboxyethylsilanetriol sodium salt (CES) is the CSDA typically applied in systems of cationic surfactant. The molecular structure of CES is also shown in Figure 3.1.

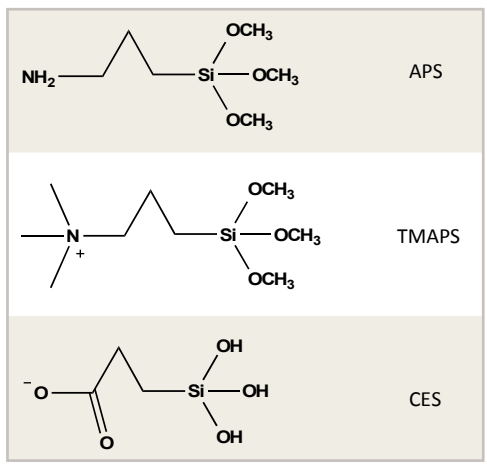

Figure 3.1. Molecular structures of CSDAs.

The CSDA interacts with the head groups of the surfactant and is co-condensed onto the silica framework. After removing the surfactant by ion-exchange extraction,[61] the non-silica part of the CSDA remains in the pores. Hence, functionalized MSMs can be achieved by a one-pot synthesis through the CSDA route. Furthermore, chiral mesoporous silicas (CMSs) have been produced via the CSDA approach by using a chiral

anionic surfactant. The CMSs usually have a helical rod-like morphology with twisted, 2D-hexagonal mesochannels. A series of CMSs have been synthesized using various chiral and achiral surfactants and CSDAs, which opens up an extensive area for research.[23, 62]

MSMs synthesized using anionic surfactant as structure directing agents through the CSDA route are named AMS. Until now, various AMS materials, AMS-1 to AMS-10, have been synthesized using different anionic surfactants and CSDAs under appropriate synthesis conditions. Table 3.1 summarizes the synthesis and structural information for typical AMS materials.

Table 3.1. Structural and synthesis information for AMS-n materials.[60, 63-65]

	Structure	Surfactant*	CSDA	Example Conditions
AMS-1 [60]	3D-hexagonal *P*6$_3$/*mmc*	C_{14}GluS	TMAPS	Molar ratio TMAPS/C_{14}GluS=2, TEOS/C_{14}GluS=12–15 pH around 9
AMS-2 [60]	Modulated *Pm*$\bar{3}$*n*	C_{12}GluA	APS	Molar ratio APS/C_{12}GluA=2–8, TEOS/C_{12}GluA=15–21 pH around 9
AMS-3 [60]	2D-hexagonal *p*6*mm*	C_{16}AS	TMAPS	Molar ratio TMAPS/C_{16}AS=1, TEOS/C_{16}AS=7.5–10 pH around 9
AMS-4 [60]	Cubic and hexagonal	C_{12}AlaA	APS	Molar ratio APS/C_{12}AlaA=0.75–1, TEOS/C_{12}AlaA=6–7.5 pH around 9
AMS-5 [60]	Lamellar	C_{12}AlaA	APS	Molar ratio APS/C_{12}AlaA=1, TEOS/C_{12}AlaA=3–5 pH = 9.4
AMS-6 [63]	Bicontinuous cubic *Ia*$\bar{3}$*d*	C_{12}AlaA	APS	Molar ratio APS/C_{12}AlaA=0.75, TEOS/C_{12}AlaA=6.75 pH = 5
AMS-7 [63]	3D-disordered	C_{14}GluSA	TMAPS	Molar ratio APS/C_{14}GluSA=1.5, TEOS/C_{14}GluSA=16.5 pH around 9
AMS-8 [63]	Cubic *Fd*$\bar{3}$*m*	C_{12}GlyS	TMAPS	Molar ratio APS/C_{12}GlyS=1, TEOS/C_{12}GlyS=10 pH = 8.8
AMS-9 [64]	Tetragonal *P*4$_2$/*mnm*	C_{12}GluA	APS	Molar ratio APS/C_{12}GluA=2.5, TEOS/C_{12}GluA=11.8 pH = 9.3, time dependence
AMS-10 [65]	Bicontinuous cubic *Pn*$\bar{3}$*m*	C_{12}GluA	TMAPS	Molar ratio TMAPS/C_{12}GluA=1.5, TEOS/C_{12}GluA=15 pH around 5

* A: Free acid, S: Sodium salt, Glu: L-glutamic acid, Ala: L-alanine, Gly: glycine

Mesostructures of AMS have been described as being easily controlled by varying the ionization degree of the anionic surfactant, for instance by simply controlling pH. One example is the materials synthesized using *N*-myristoyl-L-glutamic acid (C_{14}GluA) as the template and TMAPS as the CSDA, published by Gao et al. in 2008.[66] A full-scale synthesis-field diagram was obtained by varying the C_{14}GluA-NaOH-TMAPS composition ratios. Using a molar ratio of TMAPS to C_{14}GluA as 1.5:1, the mesostructures were changed from *Pn*$\bar{3}$*m* structure (AMS-10) to *p6mm* structure (AMS-3), to *Fd*$\bar{3}$*m* structure (AMS-8) and then to tetragonal $P4_2/mnm$ structure (AMS-9) through the successive addition of NaOH.[65] With the molar ratio of TMAPS to C_{14}GluA being 2:1, and as the concentration of NaOH increases, the structure changes from the *Pn*$\bar{3}$*m* structure, to the *p6mm* structure, to the *Fd*$\bar{3}$*m* structure, and finally to the *Fm*$\bar{3}$*m* structure.[66] In the reported synthesis system, the concentration of C_{14}GluA, a weak acid, was a fixed parameter, and the quaternary ammonium site in TMAPS is pH independent, thus controlling the pH is directly related to addition of NaOH. Figure 3.2 shows a structure diagram for this system depending on pH and addition of TMAPS (reproduced from Gao's work).[66]

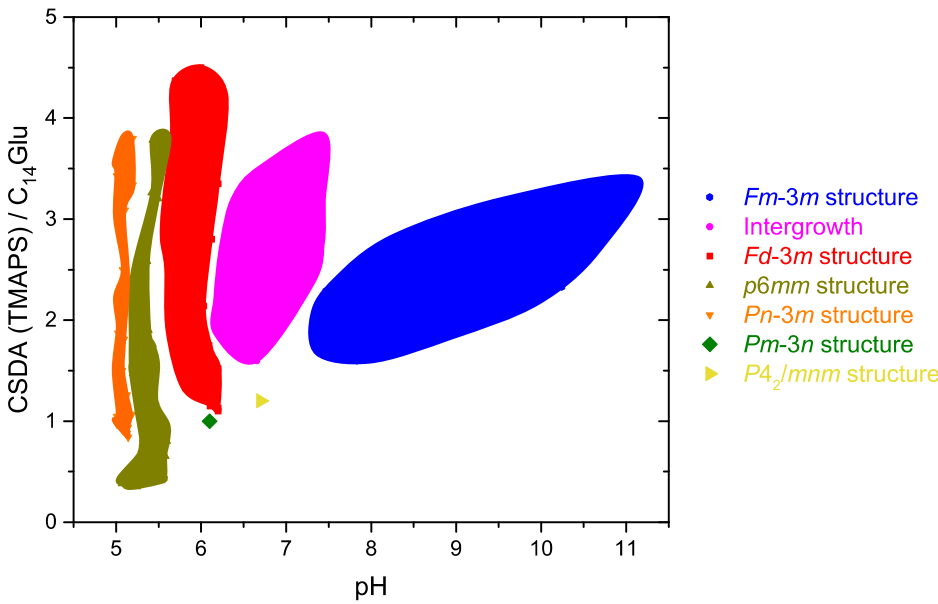

Figure 3.2. Synthesis structure diagram of the C_{14}GluA/NaOH/TMAPS system, pH vs. molar ratio TMAPS/C_{14}GluA (reproduced from ref. [66]).

The control of the organic/inorganic interface curvature has been suggested as an explanation of the structural variation influenced by pH in this system. It was explained that the interface curvature could be influenced by the ionization degree of the anionic surfactant that will affect the electrostatic interactions between the surfactant head group and the CSDA. Gao et al. have summarized the influence of the properties of the surfactant and the CSDA in the CSDA approach.[59] They have investigated the syntheses of AMS by changing the geometry of the surfactant itself, such as different chain length and/or changing head groups.[67] It has been observed that the final structures and the pore characteristics can be understood from the architecture of the surfactant. Additionally, CSDAs with different sizes of the non-silica part, for instance from the amino group to the methylamino group, the dimethylamino group and the trimethylammonium group, have been introduced to the synthesis as well. It was concluded that CSDA is present on the outside of the micelles serving as a counterion that affects the interface curvature, since the structure of the final product changes towards lower packing parameters when the size of the non-silica group of CSDA increases.[67] Moreover, the kinetics of formation of MSMs using the CSDA method is suggested to play a very important role in the synthesis.[59]

The formation mechanism of mesoporous silica is a topic of on-going discussion. For instance, the structure variation reported in one synthesis system can be simply controlled by pH but still require further investigation for a complete understanding. Most of the studies have been performed by investigating the properties of the final MSM products, however more investigations need to be conducted to understand the mechanisms of the CSDA strategy during the synthesis, from the starting solution to the final product, which should involve more detailed and systematic analysis of the intermediate products in the synthesis.

We are interested in shedding more light on the mechanism of the formation process used in the CSDA approach, and, in this thesis work, two synthesis systems are investigated: system 1, synthesis of carboxylic group functionalized MSM using a divalent cationic surfactant as template and CES as CSDA, and system 2, synthesis of CMS using a surfactant with an alanine head group as template and APES as CSDA.

3.1 System 1: synthesis of MSM using cationic surfactant and anionic CSDA

As introduced above, the CSDA method that was designed for the synthesis using anionic surfactants can also be applied to synthesis using cationic surfactants. If the anionic surfactant and the CSDA used in the synthesis of AMS, reverse the sign of the respective

charges, corresponding cationic-surfactant templated MSMs are produced. The feasibility of this approach was first demonstrated by Han and co-workers, in 2007, using CES (Figure 3.1) as the CSDA.[68] The CSDA in these cationic-surfactant-templating systems is somehow indispensable even though MSMs can be formed through the common, and simple, strategy without addition of CSDA. Compared to conventional synthesis, the mesostructures of those materials prepared by the CSDA route are diverse, and can be easily changed and controlled by adjusting pH. Highly ordered mesostructures can be formed even under neutral or weakly acidic pH (= 5–8) conditions when following the CSDA route. Under these conditions no mesostructure could be achieved conventionally. Additionally, functionalized MSMs with anionic functional groups can be obtained in a one-step synthesis using the CSDA route.

Han et al., using this one-pot CSDA approach, synthesized carboxylic group functionalized mesoporous silica using different types of cationic surfactants.[68] One of the cationic surfactants was a divalent surfactant, octadecylpentamethyl-1,3-propylenebis (ammonium bromide), $C_{18}H_{37}N^{+}(CH_3)_2(CH_2)_3N^{+}(CH_3)_3Br_2$ (designated as $C_{18\text{-}3\text{-}1}$, Figure 3.4). It was observed that, with increasing concentration of HCl, a mesostructure transformation took place. Low concentration of HCl (synthesis at high pH, above 8.5) resulted in a material consisting of a mixture of CCP, $Fm\bar{3}m$ structure, and HCP, $P6_3/mmc$ structure. High concentration of HCl (synthesis at pH below 7.5) resulted in the $Fd\bar{3}m$ structure. An intermediate concentration of HCl resulted in a gradual transformation from the $Fm\bar{3}m$ (mixed with $P6_3/mmc$) to the $Fd\bar{3}m$ structure.[43] The material with HCP or CCP structure contains spherical cavities, whereas those with the $Fd\bar{3}m$ structure have polyhedral cavities.[43, 69] Figure 3.3 shows the SAXD patterns of as-synthesized materials reproduced from Han's work including the pH conditions of the syntheses.

The structural transformation has been suggested to occur as a consequence of the ionization degree of the CSDA.[68, 70] The CSDA contains a carboxylic group, which typically has a *pKa* in the range of 1–5. Avariation in pH was therefore suggested to influence the strength of the electrostatic interaction between the surfactant head group and the carboxylic group of the CSDA, as a consequence of the varying ionization degree of the CSDA. It was also suggested that the formation of $Fm\bar{3}m$ and $P6_3/mmc$ structures is based on packing of hard spheres, whereas a weak interaction between the CSDA and the surfactants at near-neutral pH conditions, results in packing of "soft-cages",[70] the $Fd\bar{3}m$ structure. The concept of soft cages was introduced to describe that the system was flexible, allowing the spheres to rearrange into polyhedra.

However, as stated in chapter 2, the rate of the TEOS reactions varies to a great extent in this pH range (Figure 2.2). The hydrolysis rate of TEOS reaches a minimum at a pH around 7. The condensation on the other hand shows a reverse behavior with the highest rate just around pH 8.[30, 32] It is important to note that at a pH around 7, where the hydrolysis rate of TEOS is low, the $Fd\bar{3}m$ structure is formed. Hence, a complicating

aspect in this system is the variation in kinetics of the reactions involving the silica source.

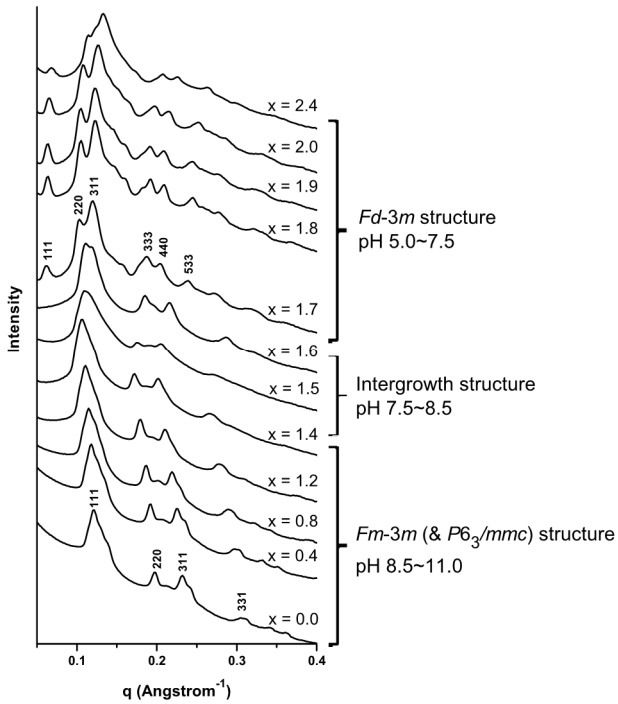

Figure 3.3. SAXD patterns of carboxylic group functionalized MSMs with the final composition, $C_{18\text{-}3\text{-}1}$: 2CSDA: xHCl: 15TEOS: 2000H_2O (x = 0.0–2.4), along with the corresponding pH values.

In order to understand the origin of the structural control in the formation of this synthesis, detailed investigations have been done both on the surfactant in pure water solution (summarized in Paper I), and on the synthesis process (summarized in Paper II, III and IV).

In the study of the synthesis process, the effects of kinetics on the formation and cross-linking of silica of the $Fm\bar{3}m$ (intergrown with $P6_3/mmc$) structure and the $Fd\bar{3}m$ structure have been investigated and summarized in Paper II. In paper III, sodium chloride is added into the same system and its influence on the materials is explored. Finally in Paper IV, the role of CSDA is discussed and the understanding of the formation mechanism for this synthesis system is further related to a reversed AMS system. The surfactants and the CSDAs involved in these two systems are shown in Figure 3.4. The main results and conclusions for the synthesis of carboxylic group functionalized mesoporous silica are discussed in chapter 5.

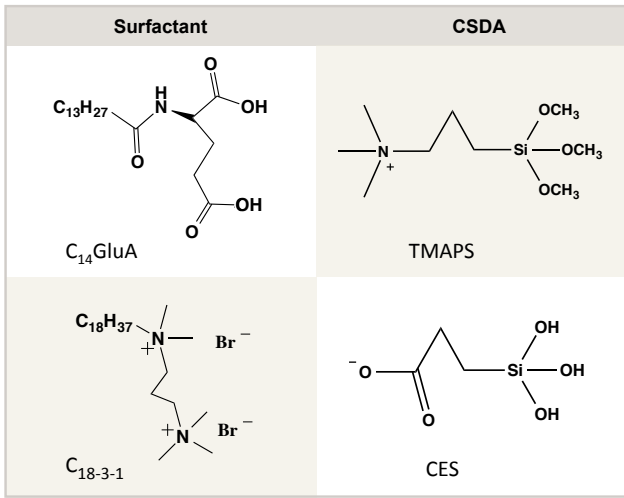

Figure 3.4. The surfactants and CSDAs of two revised synthesis systems.

3.2 System 2: synthesis of chiral mesoporous silicas

Chirality is commonly found in nature. It is an inherent feature of the molecular and macromolecular components in organisms. Producing chiral materials, and understanding the rules that govern their formation, are important endeavors in scientific research especially since chiral molecules contribute greatly to the fields of pharmacy, biochemistry, optical devices, etc.

Compared with chiral structures occurring in organisms, chirality is harder to impose on inorganic materials.[62] A facile approach to solving this problem is to involve organic chiral elements in inorganic systems, such as using organics as templates. Hence, by using chiral molecules, the strategy of synthesizing MSMs can be used to produce chiral inorganic materials with highly ordered mesostructures. Among them, chiral mesoporous silicas (CMSs) have been produced by Che et al. since 2004.[62, 71]

CMS typically exhibits a novel helical mesostructure with hierarchical chirality transcribed from the organic templates and represents a new fashion for the design and application of inorganic chiral materials. Like MSMs, CMSs have been synthesized by cooperative self-assembly of chiral amphiphiles (resulting in one chirality) and the silica species.[62] In fact, even achiral amphiphiles have been found to produce CMSs, but the morphology then as a "racemic" mixture. For cationic surfactants, the formation is based on the positive interactions between the head groups of surfactants and the inorganic reagents as mentioned in previous chapters. For anionic surfactants, CSDAs are applied

to induce favorable interface interactions; for instance, the positively charged ammonium ion of a CSDA, such as APS or TMAPS, interacting with the negatively charged head group of anionic surfactants.

In the family of anionic surfactants, a chiral surfactant is normally an amino acid-derived surfactant. Amino acid-derived surfactants are readily obtained by reactions of amino acids with alkyl acyl chloride under basic conditions in aqueous solutions, followed by acidification and recrystallization.[72] Some amino acid-derived surfactants have been commercialized and can be purchased from chemical suppliers.

Morphology control of CMS is also a widespread topic of research, as the chirality within the individual molecules can be expressed in larger-scale structures. Materials with different morphologies can have different properties and be applicable for different uses. CMSs do not always have a helical rod-like morphology, but can also have other morphologies such as helical ribbons or helical tubes. Different morphologies of mesoporous silica have been obtained when using the same chiral surfactant as the structure directing agent, under different synthesis conditions. In other words, the formation of CMS is extremely sensitive to the synthesis conditions. CMSs of diverse sizes and shapes have been synthesized by precise control of the reaction composition and experimental parameters, such as temperature, pH and even stirring rate.[73]

It was found that, by using *N*-myristoyl alanine (C_{14}-Ala) as structure directing agent and 3-aminopropyltriethoxysilane (APES) as CSDA (Figure 3.5), mesoporous silica with four different morphologies can be synthesized just by controlling the synthesis temperature to 0, 10, 15, and 20˚C respectively. The morphologies obtained were helical ribbons, hollow spheres, circular disks, and helical rods.

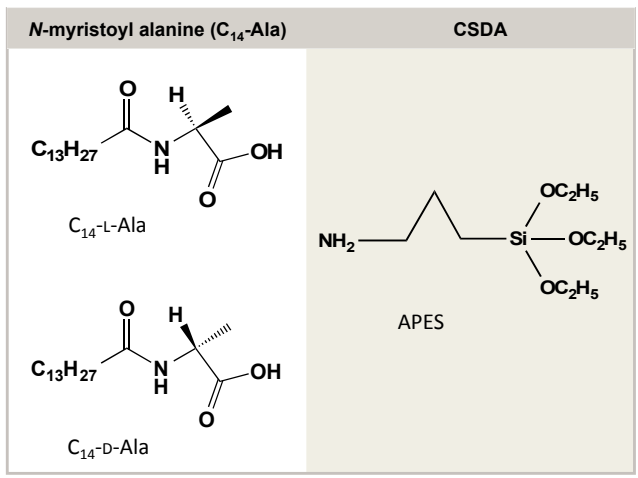

Figure 3.5. Chemical structures of *N*-myristoyl alanine surfactant and APES.

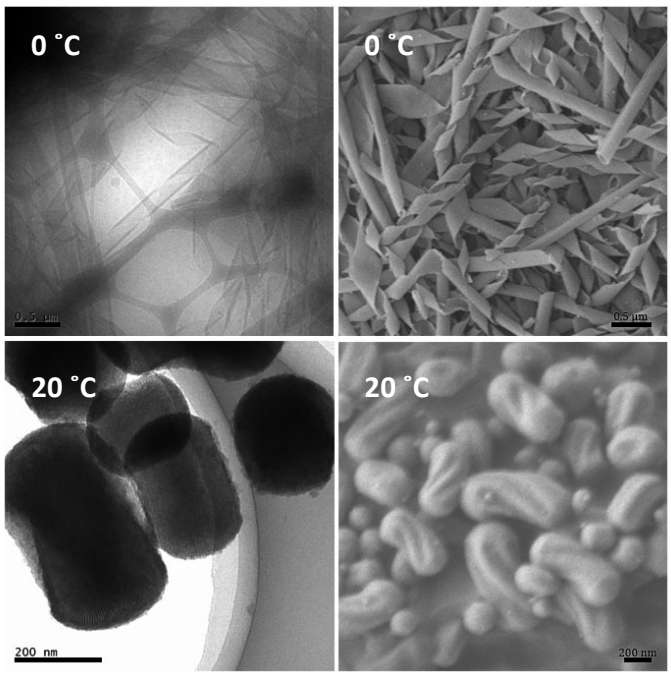

Figure 3.6. TEM (left) and SEM (right) images of mesoporous silicas synthesized at 0 ˚C and 20 ˚C.

The mesoporous silica helical ribbons are uniform in handedness, i.e., completely right-handed when the L-form *N*-acyl amino acid (C_{14}-L-Ala) is used. However, the corresponding helical rods that are synthesized using the same surfactant are predominantly left-handed.[74] SEM images of these two types of materials are shown in Figure 3.6. The materials are reproduced according to reference [74]. These findings give important hints for the understanding of the formation of chiral materials at the molecular level. For instance, the chiral senses of the *N*-acyl-amino acid molecules in the lamellar structure of the helical ribbon may be expressed differently than in the rod-like helical channels, and thus result in different chiral assemblies. Nevertheless the mechanistic details are not yet fully understood.

The formation of helical ribbons at 0˚C is a slow process, which makes it possible for us to follow the synthesis more or less continuously. Paper V summaries the investigation on the synthesis of helical ribbons using the *N*-myristoyl-L-alanine (C_{14}-L-Ala) surfactant as structure directing agent and APES as CSDA. The main results of this investigation are summarized in Chapter 6.

4 Main Methodology

In order to analyze the morphology, porosity and structure of mesoporous materials, the following experimental techniques are used in this PhD project: scanning electron microscopy (SEM) is used to get information about the morphology and the size of the mesoporous silica particles;[75] gas adsorption measurements are used to obtain the surface area and the pore size distribution of the materials;[76] small angle X-ray diffraction (SAXD) and transmission electron microscopy (TEM) are used to identify the meso-structures of the materials.[77] Further, addition techniques that provide information on the characteristics of the ongoing synthesis, such as NMR and cryo-TEM are also used. In the work presented in this thesis, SAXD is the most commonly used technique to determine the structures of the materials. Electron microscopy is used to provide additional structural information. ^{29}Si NMR was used to investigate the silica cross-linking degree and ^{13}C NMR was used to study the behavior of the surfactants and the CSDAs during the synthesis. Furthermore, in order to understand the formation of the MSMs, the binary surfactant/water system has been investigated using small angle X-ray scattering (SAXS), dynamic light scattering (DLS), and conductivity measurements.

In this Chapter, overviews of the main techniques used in this thesis work are provided.

4.1 Small Angle X-ray Scattering (SAXS)

SAXS is generally used as an analytical method to investigate particle systems in terms of averaged particle sizes and shapes. Normally, when X-rays penetrate the sample, the particles located inside the volume that the beam passes through will produce scattering, as they have different electron density from the solvent, and their size are in the range of the X-ray wavelength. The outgoing scattering rays produce interference patterns that are

recorded by a detector. As shown in Figure 4.1, the interferences depend on the observation angle 2θ, the orientation and the distance r between two particles.

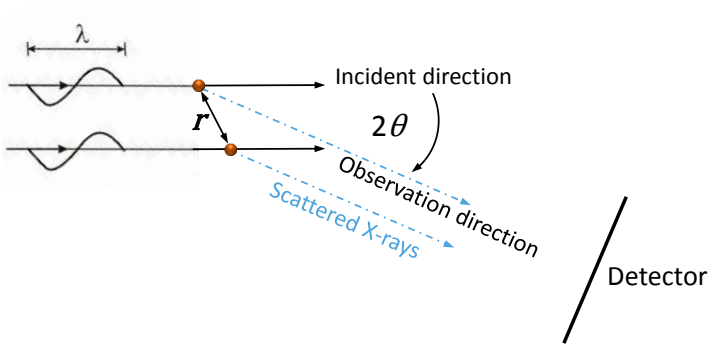

Figure 4.1. The detected waves depend on the distance r between the particles and on their orientations with regard to the directions of incidence and observation.

The distance r is measured relative to the wavelength λ of the applied X-ray. An identical value of r/λ ratio gives rise to the same interference pattern. Hence the scattering pattern is usually presented as a function of the length of the scattering vector, q,

$$q = \frac{4\pi}{\lambda} \cdot sin\theta \qquad (4.1)$$

The dimension of q is one over length (i.e. $Å^{-1}$).

In order to observe a SAXS signal of the particles, the electron density of the particles must be different from their environment, which for instance can be the solvent of a solution. The signal visibility increases with the difference in electron density between the solvent (environment) and the solute (particle). This is the so-called contrast. When a particle with the electron density of ρ_1 is in an environment having the electron density ρ_2, then the scattered intensity of the particle is

$$\Delta I_1(q) = I_0 \cdot (\rho_1 - \rho_2)^2 \cdot V_1^2 \cdot P(q) \qquad (4.2)$$

where V_1 is the particle volume, and $P(q)$ is the form factor of the particle, which bears the shape and the internal density distribution of the particles. Additionally, an ensemble of many identical particles causes an intensity of

$$\Delta I(q) = N \cdot \Delta I_1(q) \cdot S(q) \qquad (4.3)$$

where N is the number of particles, and $S(q)$ is the structure factor, which carries information about the particle to particle interactions.

When equation 4.2 and equation 4.3 are combined, it results in:

$$\Delta I(q) = K \cdot P(q) \cdot S(q) \qquad (4.4)$$

This equation (eq. 4.4) presents the information that can be obtained after background subtraction of the recorded intensity. All the constant terms are lumped together into K, which consists of the contrast, the volume, and the concentration of the particle. The other factors, $P(q)$ and $S(q)$, have values that depend on the angle. They are introduced below.

4.1.1 The form factor

The scattering of one particle, consisting of many atoms, can be explained as the interference pattern produced by all the waves that are scattered from every electron/atom in the particle. This scattering pattern is characteristic for the shape of the particle, and is therefore called "the form factor", $P(q)$.

Generally, in a dilute sample, where the particles are far away from each other, and the particles are all identical in shape and size, the experimental scattering pattern is the form factor multiplied by the number of particles that happen to be in the X-ray beam. Every particle produces a form factor that is characteristic of its shape. At small angles (low q), the character of the form factor is determined by the overall size. At large angles, the character of the form factor gives information about the surface. In the middle part, which is also the oscillation part, the shape, such as globular (spherical), cylindrical and lamellar shape, and the internal density distribution of the particles are displayed.

The oscillating part of the form factor is described by transforming it into real space,

$$P(q) = 4\pi \int_0^\infty p(r) \frac{\sin(qr)}{qr} dr \qquad (4.5)$$

This equation is based on a so-called "pair-distance distribution function" (PDDF), p(r).[78] This function provides a histogram of distances that can be observed inside the particle, and it can have different profiles depending on the particle's architecture. It is also possible to detect a difference in electron density within a particle, for example in a core-shell particle (Figure 4.2). The contrast in ordinate is presented by $\Delta\rho$. If the contrast of the environment is subtracted as 0, when the contrast of the core is smaller than that of the environment, the $\Delta\rho$ of the core is negative.

It is worth mentioning that in SAXS experiments, the shape of the form factor is the average of all the illuminated particles in the sample. The $P(q)$ is therefore typically the sum of particles with different shapes (polymorphous) and different sizes (polydisperse), weighted with the respective contrast and volume. Hence, polydispersity should be taken into consideration during the data analysis.

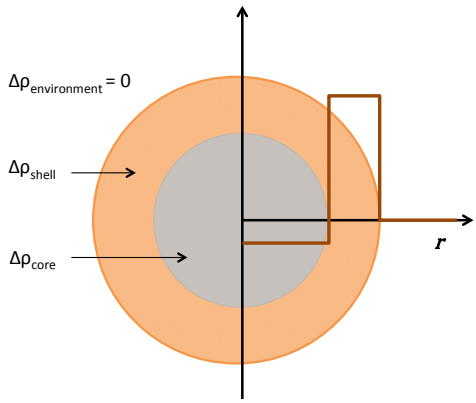

Figure 4.2. Electron desity profile of a core-shell particle.

4.1.2 The structure factor

When particle systems are densely packed, for instance in a concentrated surfactant/water system, the distances between particles is close to the same value as the size of the particles. The interference pattern will therefore contain contributions from neighboring particles as well. This additional interference pattern is called "the structure factor", $S(q)$.

The structure factor multiplied with the form factor of the single particle provides the overall interference pattern. In the case of a dilute system, where only $P(q)$ is involved (eq. 4.2), the approximation $S(q) = 1$ holds. In systems where the particle shape can change with the concentration, for instance for surfactants in aqueous solution, the structure factor $S(q)$ cannot be neglected. Including the structure factor means that the inter-particle forces are taken into account, and they affect mainly the low-q region of the scattering pattern. The strength of the interaction depends on the concentration of the particles and the force they exert on each other. The well-known interaction (force) types are hard-sphere interaction, coulomb interaction and van-der-waals interaction. Typically, a repulsive interaction leads to a decrease in intensity, and attractive interaction results in an intensity increase.

When the particles align into a highly ordered and periodic arrangement, the SAXS pattern will give rise to peaks. The peaks are called Bragg peaks. The peak positions give a fingerprint of the structure. This crystalline case is introduced more in the next SAXD section.

4.1.3 Data analysis

Before the data analysis, the measured SAXS pattern needs to be brought to absolute scale by subtracting the background. This is done in three parts: (1) clean the data from the dark-count rate of the detector, $I_{dc}(q)$; (2) scale the curves by their respective transmittance values, T_x; and (3) subtract the environment (solvent and sample holder) from the sample (particle). These three steps can be summarized in one equation:

$$\Delta I(q) = \frac{I_{sample}(q) - I_{dc}(q)}{T_{sample}} - \frac{I_{environment}(q) - I_{dc}(q)}{T_{environment}} \tag{4.6}$$

In addition, in order to calculate the absolute intensity, $\Delta I(q)$ needs to be related to a reference absolute intensity, for example, water at 20°C has $I = 1.64 \times 10^{-2}$ cm^{-1}. Hence in aqueous solution, the absolute intensity is described as

$$\Delta I_{abs}(q) = \frac{\Delta I(q)}{\langle \Delta I_{water} \rangle_q} \cdot I_{water,ref} \tag{4.7}$$

In this thesis work, SAXS is used to investigate the divalent ionic surfactant ($C_{18\text{-}3\text{-}1}$)/water system. After the data are brought to absolute scale by subtracting solvent and capillary contributions, they are fitted by SasView[79] 3.1.2. Since surfactant's counterion Br^- has a high electron density, and they condensed on the micellar surface, the form factor was fitted using the core shell model described with the following equation,[80]

$$P(q) = \frac{scale}{V_s}\left[3V_c(\rho_c - \rho_s)\frac{sin(qr_c) - qr_c cos(qr_c)}{(qr_c)^3} + 3V_s(\rho_s - \rho_{solv})\frac{sin(qr_s) - qr_s cos(qr_s)}{(qr_s)^3}\right]^2$$

where scale is a scale factor, V_c is the volume of the core, V_s is the volume of the shell, r_c is the radius of the core, r_s is the outermost radius of the micelle ($= r_c +$ shell thickness), ρ_c, ρ_s and ρ_{solv} are the scattering length density (SLD) of the core, the shell, and the solvent, respectively.

Since the system of divalent ionic surfactant is highly charged, the Hayter structure factor model, which is based on coulomb interaction, was used.[81-82] The parameters involved in the structure factor fitting are effective radius (the outermost radius), charge, volume fraction, temperature, and dielectric constant.

4.2 Small Angle X-ray Diffraction (SAXD)

The SAXD technique can be used to obtain structural information about ordered materials with a structural order in the size region of 1–100 nm. Typically, since crystals are ordered 3-D periodic structures, the interaction between an X-ray beam and an array of planes of atoms will give rise to diffraction. The diffraction pattern is the characteristic of the structure in the crystal.

The X-ray diffraction is based on the interference of the X-ray beams being reflected from the planes of atoms within the crystal at specific orientations. Depending on structure and orientation the reflected beams may reinforce, giving rise to constructive orientation, or cancel out. By recording the reflected beams, a "fingerprint" of the structure is obtained. SAXD generally relies on powder pattern of the sample, just like XRD, which means that a large number of particles or ordered domains contribute to the scattering pattern. The scattering gives rise to a ring pattern, which is typically presented in a diagram where the intensity is shown as a function of 2θ (or $1/d$ or q).

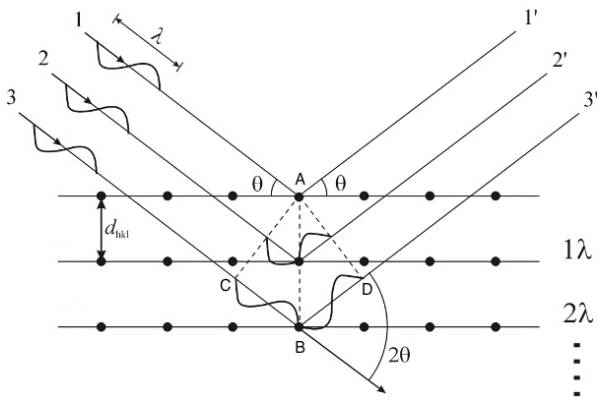

Figure 4.3. Schematic illustration of the reflection of X-rays from a set of crystal planes.

Figure 4.3 is a simple schematic explaining the reflection of X-rays by planes of atoms in a crystal. In the figure, the array of atoms (black dots) represents a section through a crystal. The lines that link the dots mark one set of parallel planes with an interplanar spacing d. The X-rays with a wavelength λ, marked as 1, 2, 3, hit the planes at an angle θ. Ray 1 is scattered by the atom at A and ray 3 is scattered by the atom at B. For constructive interference to occur of the reflected beams, the path length difference of the interfering beams, here for example ray 1 and ray 3, must be equal to an integral number of wavelengths. If AC and AD are drawn at right angles to ray 3, the difference in path length between the two beams, ray 1 and ray 3, is given by:

difference in path length = CB + BD

here

$$\text{CB} = \text{BD} = d\sin\theta$$

As explained above, the difference in path length must be equal to an integer number, n, of wavelength λ in order for constructive interference to occur. The

$$\text{difference in path length} = 2d\sin\theta = n\lambda$$

This condition is summarized in Bragg's equation:

$$n\lambda = 2d\sin\theta \tag{4.8}$$

Equation 4.8 with different values of n specifies the same group of crystal lattice planes. So the Bragg's equation can be simplified without n as

$$\lambda = 2d\sin\theta \tag{4.9}$$

In this thesis the SAXD results are presented as a figure of the intensity as a function of the scattering vector q. The relation between q and d is shown in equation 4.10.

$$d = 2\pi/q \tag{4.10}$$

In order to define the different sets of parallel lattice planes, Miller indices ($h\ k\ l$) are used for the description of the planes and directions.[83] The triplet Miller indices, h, k, and l, are three integer components without any common denominator. $\langle hkl \rangle$ can be seen as a vector perpendicular to a plane in the lattice space, and this set of planes can be characterized as (hkl). The Miller indices are related to the interplanar spacing d, but the relationship is different in different crystal systems. For instance, the relation between d and the Miller indices for a cubic crystal system is

$$\frac{1}{d^2} = \frac{h^2+k^2+l^2}{a^2} \tag{4.11}$$

and for a hexagonal crystal system:

$$\frac{1}{d^2} = \frac{4}{3}\left(\frac{h^2+k^2+l^2}{a^2}\right) + \frac{l^2}{c^2} \tag{4.12}$$

where a and c are the unit cell parameters.

The measured SAXD patterns, based on the scattering vector q, can be indexed with the Miller indices, hkl, by the relations, for example,

$$q \propto \frac{1}{d} \propto \sqrt{h^2 + k^2 + l^2} \tag{4.13}$$

for a cubic crystal system. The lattice spacing can be calculated when hkl is determined.

In this thesis work, when the SAXD pattern is complicated, analytical softwares are used to help index the pattern. These softwares are Jana2006,[84] WinXPOW,[85] and GSAS II.[86]

4.3 Electron Microscopy

Microscopy is a technique that makes it possible to see objects, which are too small to be seen by the naked eye. The well-known optical microscope uses visible light and a system of optical lenses to enlarge images of small objects. Unlike the optical microscope, an electron microscope instead uses a beam of accelerated electrons as a light source and a system of electromagnetic lenses. Thanks to the fact that electrons can be deflected in a magnetic field, an electron microscope can enlarge small objects with a higher resolution than the light microscope.

Imaging with electron microscopy is based on the interactions between the electron beam and the atoms of the specimen. As shown in Figure 4.4, when the accelerated electrons hit a sample, various reactions can happen, such as electrons being scattered either as elastic scattering or inelastic scattering. The elastic scattering of the incident beam causes diffraction and can generate backscattered electrons. The inelastic scattering results in the emitting of secondary electrons, auger electrons, characteristic X-rays, diffraction and visible light from the target sample. The secondary and backscattered electrons, recorded on the topside of the specimen, are utilized in Scanning Electron Microscopy (SEM), where the electron beam is scanned over the specimen providing information on the surface. In Transmission Electron Microscopy (TEM), the electrons pass through a thin sample and are recorded in the bottom of the microscope.

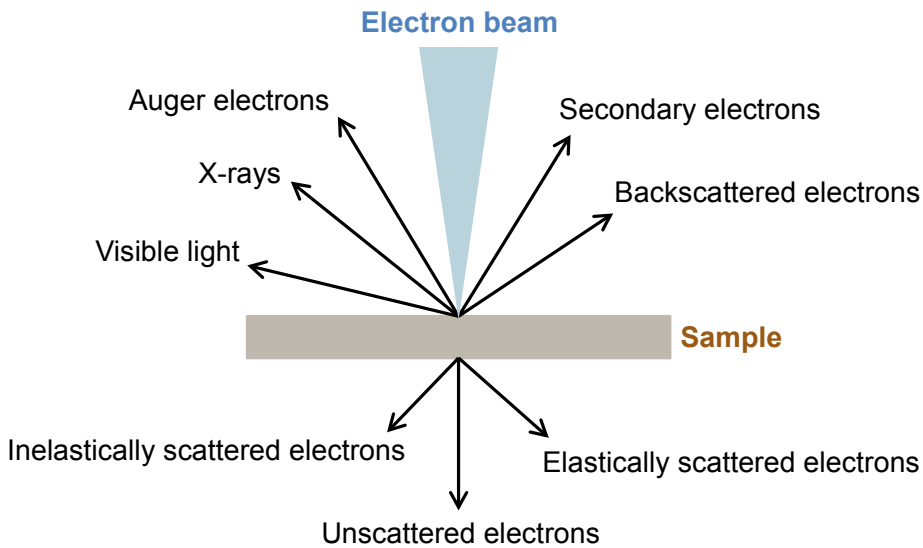

Figure 4.4. Different types of resulting interactions when the electron beam hits a sample.

4.3.1 Transmission Electron Microscopy (TEM)

As mentioned above, TEM is used to investigate a thin specimen by detecting the electron beam that is transmitted through the specimen. The electrons transmitted through the specimen – elastically scattered, inelastically scattered and unscattered (i.e. the primary beam) electrons – can form a diffraction pattern or an image, depending on what the operator chooses. Typically the elastically scattered electrons carry the most easily interpretable information of the sample. The image is magnified, focused and recorded onto an imaging device.

Figure 4.5 shows the basic optical components in a TEM. A TEM instrument can be described as being partitioned into three systems: illumination system, objective lens/stage system, and imaging system. The illumination system is used to produce, accelerate and focus the incident energetic electron beam onto the sample. The sample holder is involved in the second system, where the interactions between the incident electrons and the specimen take place, and the diffraction and image are formed. The objective lens is the heart of the microscope and forms the image. In the imaging system, the strength of the intermediate and projector lenses is controlled, whereby the magnification of the diffraction pattern or the image can be chosen. The image or diffraction pattern is projected onto the screen or recorded with the camera.

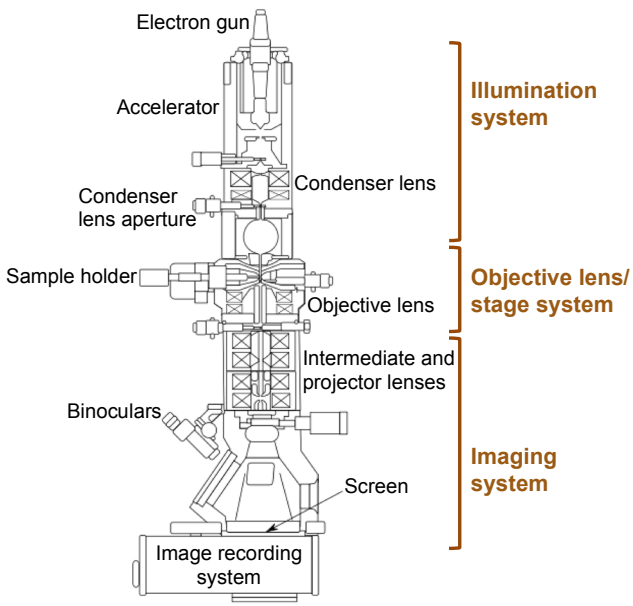

Figure 4.5. Schematic of basic optical components in a TEM.

In this thesis, we use TEM to ascertain particle size and morphology of the materials. We also obtain structural information. The contrast in a TEM can simply be described as caused by either amplitude contrast or phase contrast. Amplitude contrast, or mass-thickness contrast, arises as the extent of transmission of unscattered electrons. Areas of the specimen that are thicker or contain heavy elements will have fewer transmitted electrons and will appear darker, and, conversely, the thinner areas will have more transmitted beams and will thus appear lighter. Phase contrast is created as the unscattered beam interferes with the scattered beams, in the same way as the interference pattern caused X-rays. One important difference between X-rays and electrons is that electrons are scattered much more easily than X-rays, which can complicate the interpretation of an electron diffraction pattern. A big advantage to electrons however is that they can be deflected inwards by an electromagnetic lens and an image can be formed. The phase contrast is most easily interpreted when the scattering object is thin. The materials investigated in this thesis consist of SiO_2 and the contrast variation is generated by the fluctuating mass-thickness contrast of the pore system but also form phase contrast due to the ordered structure.

4.3.2 Cryogenic Transmission Electron Microscopy (Cryo-TEM)

A normal TEM has the disadvantage of being limited to dry solid samples. However, a TEM can also be equipped with additional features allowing it to work under cryogenic conditions, i.e. temperatures below -150˚C. Such a microscope is called a cryogenic TEM or cryo-TEM. Cryo-TEM makes it possible to do TEM measurements on soft matters, liquid systems and in our case, the synthesis solution of mesoporous silicas.[87-88]

In order to investigate liquid samples in a cryo-TEM, the sample must be rapidly vitrified to produce a thin film of vitreous ice on the carbon-coated copper grid. This is usually done by taking a 5 μL droplet of the sample solution and placing it on the grid under controlled environmental conditions using a vitrification system,[89] then blotting the grid with filter paper to remove excess fluid and to get a homogenous liquid film coverage of the grid, and finally rapidly plunging the grid into liquid ethane (at -180˚C) to ensure rapid vitrification of water. The carbon grid can then be stored in liquid nitrogen before insertion into the electron microscope. The cryo-TEM contains a cryogenic specimen holder that maintains the sample at liquid nitrogen temperatures. It is important to keep the temperature below -160˚C in order to prevent the formation of cubic and hexagonal ice.[90]

During a synthesis of mesoporous silica material, when we freeze the synthesis solution to prepare the grid for cryo-TEM measurements, the reaction is stopped, which provides the opportunity for us to investigate the solution at different synthesis stages.

We hence obtain snap-shots of the synthesis solution providing information on the state of the reaction/formation at that particular time.

4.4 Nuclear Magnetic Resonance (NMR)

Nuclear magnetic resonance spectroscopy, known as NMR spectroscopy, is a technique that can elucidate the chemical structure of compounds and assess their quantity. It can determine the physical and chemical properties of atoms or molecules, and hence provide detailed information about the structure, dynamics, reaction state, and chemical environment of the molecules. It is also routinely used in advanced medical imaging techniques, such as magnetic resonance imaging (MRI).
NMR is a physical phenomenon that nuclei in a magnetic field absorb energy and give rise to electromagnetic radiation. This energy is at a specific resonance frequency and depends on the strength of the magnetic field and the magnetic properties of the nucleus,[91] according to the Bohr frequency condition:

$$\Delta E = hv \tag{4.14}$$

where v is frequency of electromagnetic radiation and h is Planck's constant. ΔE describes the energy difference between the energy levels.

NMR uses a property of the atomic nuclei called the nuclear spin, which is equivalent to small magnetic fields. Nuclei that contain an odd number of protons and/or neutrons have a nonzero spin, whereas with even numbers of both they have a total spin of zero. If the sum of spins from an individual nucleus is nonzero, the nucleus will behave as a weak magnet when placed in a magnetic field. The most commonly studied nuclei are ^{1}H and ^{13}C. They both have a spin of $-1/2$ and a natural abundance of ~99% for ^{1}H and ~1% for ^{13}C. Furthermore, nuclei from isotopes of many other elements, such as ^{17}O, ^{23}Na and ^{29}Si, can also be studied by NMR.

Because of the spin property, a nucleus can be considered a small compass needle. In a strong magnetic field (B_0) the nucleus will experience a shift of energy. A low energy conforms when its spin is aligned to the field. However, as soon as a spin is not perfectly aligned along the field, a precession about the direction of magnetic field takes place. The overall magnetization can be visualized as a processing vector around the field with a frequency of ω_0. This frequency is defined by the gyromagnetic ratio of a nucleus, γ, and the strength of the external magnetic field, B_0, and is called the larmor frequency:

$$\omega_0 = \gamma B_0 \tag{4.15}$$

where the gyromagnetic ratio, γ, is an inherent property of the nucleus.

Different types of spins of nuclei give rise to different magnetic moments, and they differ depending on the type of element. Thus, given external field strength, it is possible to distinguish between different types of atoms.

Moreover, the electron distribution around a nucleus can screen the nuclei from the external magnetic field, which results in a slightly different resonance frequency depending on the position of an atom in a molecule. This latter effect is called chemical shift, and it enables NMR to distinguish nuclei in different chemical environments.[91] For instance, since hydrogen situated at different positions within a molecule have different ΔE, the NMR measurement gives rise to different signals. The chemical shift is normally not assigned an absolute value but is quantified relative to a reference frequency:

$$\delta = 10^6 \cdot \frac{\nu - \nu_{ref}}{\nu_{ref}} \qquad (4.16)$$

where ν is the frequency of the measured nucleus and ν_{ref} is a reference frequency. The chemical shift is usually expressed in parts per million (ppm).

Here we give an overall introduction of the usage of analysis of ^{13}C PT ssNMR and ^{29}Si NMR measurements.

4.4.1 ^{13}C Polarization Transfer solid-state NMR (^{13}C PT ssNMR)

In this thesis work, we have used ^{13}C Polarization Transfer solid-state NMR (^{13}C PT ssNMR)[92-93] to investigate the mobility of the surfactants and the CSDAs during the synthesis of MSMs. This natural-abundance ^{13}C NMR methodology was developed by Nowacka and co-workers, and it has been used previously to characterize the molecular dynamics with atomic resolution of surfactants[92-93] and lipids.[94]

PT ssNMR measurement is a combination of three separate experiments: direct polarization (DP), cross polarization (CP),[95] and refocused insensitive nuclei enhanced by polarization transfer (INEPT)[96-99] equipped with high-power proton decoupling and magic-angle spinning (MAS). CP is based on the polarization that is transferred from ^{1}H→^{13}C by using heteronuclear through-space dipolar couplings,[95] while INEPT is based on polarization transferred through-bond.[96] The DP experiment does not involve polarization transfer. The DP spectrum generally shows resonances from all carbons in the sample and acts as a reference. Information on the molecular dynamics is given by comparing the signal intensities acquired in the INEPT and CP pulse sequences, relative to the signal obtained from the DP experiment.[93] In other words, the DP spectra give semi-quantitative information about the ^{13}C present in the sample, while the CP and INEPT spectra indicate the mobility of the C-H bonds in the molecules. A high CP signal is obtained with a rigid ^{13}C and a high INEPT signal is attained from a mobile or isotropic ^{13}C.

A theoretical model for calculating the CP and INEPT intensities as a function of rotational correlation time τ_c and ^{13}C–^{1}H bond order parameter S_{CH} has been developed by Nowacka et al.[93] From this model, it is possible to distinguish different dynamic regimes. τ_c measures the rate of the ^{13}C–^{1}H bond reorientations, while $|S_{CH}|$ is the measure of the anisotropy of the ^{13}C–^{1}H bond reorientation. $|S_{CH}|$ ranges from 1 for ordered and rigid segments to 0 for segments with isotropic reorientation. Figure 4.6 (left) illustrates the calculated signal intensities for a $^{13}C^{1}H_2$ segment, adopted from [93].

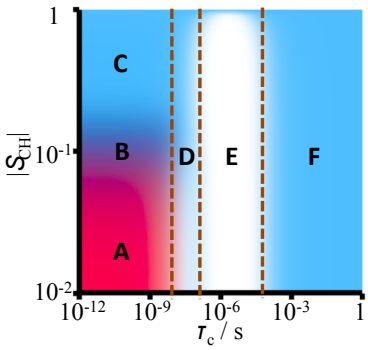

Region	Dynamic regime	τ_c	$\lvert S_{CH}\rvert$	Intensity
A B C	Fast	< 10 ns	<0.01 ≈ 0.1 > 0.5	INEPT >> CP = 0 INEPT = CP CP >> INEPT = 0
D	Fast-intermediate	≈ 0.1 µs		CP >> INEPT = 0
E	intermediate	≈ 1 µs		CP = INEPT = 0
F	slow	> 0.1 ms		CP >> INEPT = 0

Figure 4.6. Theoretical ^{13}C–^{1}H polarization transfer efficiency as a function of rotational correlation time τ_c and C–H bond order parameter $|S_{CH}|$ for a $^{13}C^{1}H_2$ segment (right). The map is color-coded according to the calculated CP (blue) and INEPT (red) intensities. White represents inefficient CP and INEPT polarization transfer. The general division of dynamic regimes is based on the tabulated values for τ_c and $|S_{CH}|$ (right). Adopted from [93].

By comparing the signal intensities acquired from CP and INEPT, the anisotropy and the dynamics of a carbon segment can be distinguished according to the values for τ_c and $|S_{CH}|$ (Figure 4.6, right). The signal enhancement is related to how the magnetization is transferred from ^{1}H nuclei to neighboring ^{13}C. When the segment has a fast isotropic reorientation ($|S_{CH}| < 0.01$ and $\tau_c < 10\ ns$), CP signals are averaged to zero. Therefore, CP is efficient in promoting signals for segments with slow ($\tau_c > 0.1\ ms$) and/or anisotropic motions. However, since non-averaged ^{1}H–^{1}H and ^{1}H–^{13}C dipolar interactions result in fast relaxation rate, INEPT will yield no signal for rigid segments with slow motion ($\tau_c > 0.1\ \mu s$) and/or highly anisotropic reorientation ($|S_{CH}| > 0.5$). On the other hand, as long as the ^{1}H and ^{13}C transverse relaxation times are longer than the time required for ^{1}H–^{13}C polarization transfer (typically in scale of ms), INEPT gives signal enhancement. Hence, spectra with high intensity of INEPT signals represent mobile segments ($\tau_c < 10\ ns$). Furthermore, for the white region in Figure 4.6 left, neither CP nor INEPT provides signal. It represents an intermediate dynamic regime with $\tau_c \approx 1\ \mu s$.

4.4.2 Solid-state ^{29}Si NMR

We have also used solid-state ^{29}Si NMR to investigate the extent of crosslinking of silica and CSDA in the as-synthesized MSMs. A typical resulting ^{29}Si NMR spectrum is shown in Figure 4.7. The silicon environment Q^4 appears around -110 ppm, Q^3 around -100 ppm, and Q^2 around -90 ppm.[100] It is also possible to determine the silica cross-linking of the CSDA. T^3, T^2 and T^1 are used to represent the cross-linking environment of CSDA: T^3 appears around -66 ppm, T^2 around -57 ppm, and T^1 around -47 ppm.[100-101] The data obtained were treated in ACD/NMR Processor Academic Edition,[102] and a Lorentzian lineshape was used to fit the peaks.

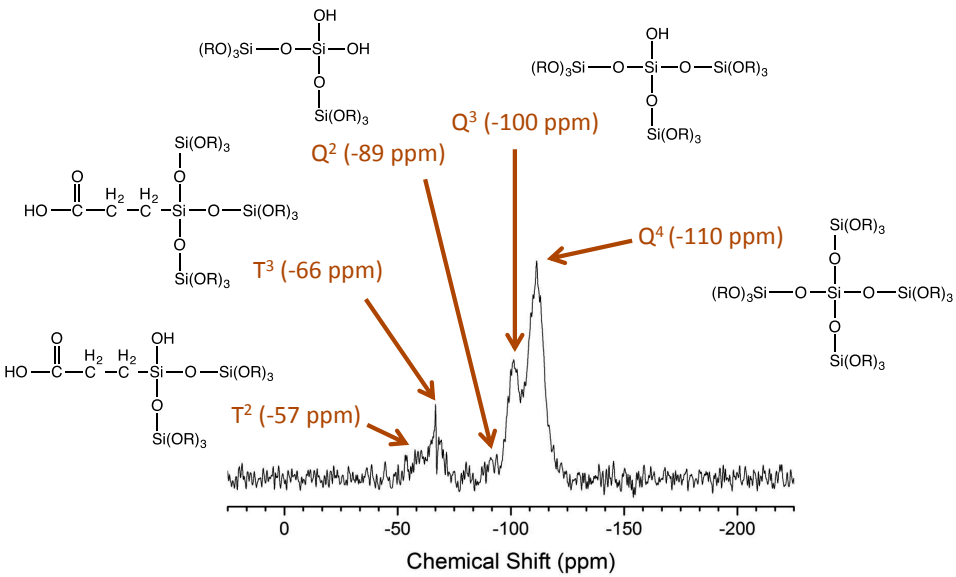

Figure 4.7. Example of ^{29}Si MAS NMR spectrum.

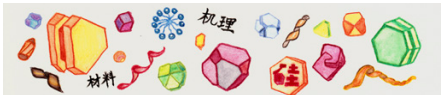

Results

5 System 1: synthesis of MSM using cationic surfactant and anionic CSDA

As mentioned in Chapter 3, carboxylic group functionalized MSMs can be synthesized using $C_{18\text{-}3\text{-}1}$ as structure directing agent, CES as CSDA, and TEOS as silica source. A structural transformation has been reported to occur as a consequence of pH. In this Chapter, we provide an insight into the structural formation and aim to understand the origin of the structural control mechanism. The results presented here are a compilation of the principal results reported in papers I–IV.

In Chapter 2, a general synthesis mechanism has been introduced. Typically, a synthesis of MSM is based on three aspect: surfactant self-assembly, silica reactions and electrostatic interaction in general. When a CSDA is introduced to the synthesis system, the synthesis environment becomes more complicated. Hence, our investigation for this synthesis system is focused on: (1) self-assembly of $C_{18\text{-}3\text{-}1}$ surfactant (Papers I and III); (2) siliceous reactions influenced by silica kinetics (Paper II); (3) investigation of electrostatic interactions by adding salt (Paper III); and (4) the role that is played by the CSDA (Paper IV). During these investigations, three structures are mainly synthesized. They are the CCP $Fm\bar{3}m$ structure, the cage-type $Fd\bar{3}m$ structure and $Pm\bar{3}n$ structure. With the aid of SAXD and PT ssNMR, a detailed investigation of the formation of these three structures from starting solution to final product has been conducted (Papers II and III). Furthermore, the mechanism concluded from this synthesis system is related to a reversed AMS synthesis system (Paper IV).

5.1 Self-assembly of $C_{18\text{-}3\text{-}1}$ surfactant in pure water and salt solutions

In order to understand the self-assembly of the $C_{18\text{-}3\text{-}1}$ surfactant in the synthesis, the simpler binary system of surfactant/water solution is studied. The results are reported in Paper I. In addition, since the electrostatic interaction is an important aspect in the synthesis of MSM, the influence of high ionic strength on the micellar architecture in a pure surfactant/salt aqueous solution is also investigated as supplemental information concerning the synthesis system of MSM.

5.1.1 $C_{18\text{-}3\text{-}1}$ surfactant in pure water

At 20˚C, $C_{18\text{-}3\text{-}1}$ is measured to have a CMC in water of 1.5 mmol/L, and a molecular volume including counterions of 829.4 $Å^3$ (Paper I). The SAXS patterns of the phase behavior of the $C_{18\text{-}3\text{-}1}$/water system are shown in Figure 5.1. The corresponding volume fractions are calculated and also shown in Figure 5.1.

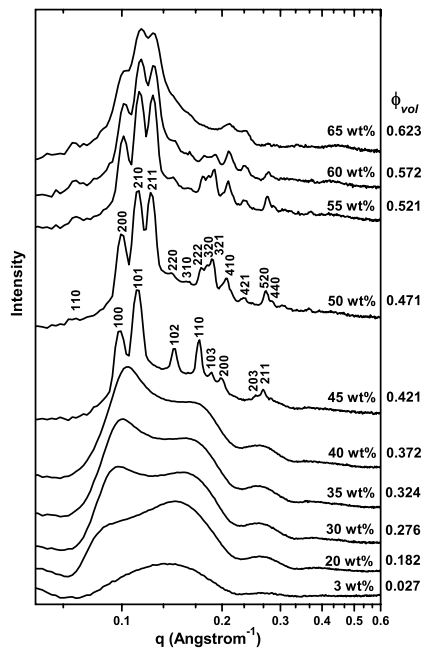

Figure 5.1. SAXS patterns of $C_{18\text{-}3\text{-}1}$ in H_2O solution at different concentrations (weight percentage and volume fraction) of $C_{18\text{-}3\text{-}1}$. The curve of 45 wt% of $C_{18\text{-}3\text{-}1}$ is indexed with the $P6_3/mmc$ structure and the curve of 50 wt% of $C_{18\text{-}3\text{-}1}$ is indexed with the $Pm\bar{3}n$ structure.

When the concentration of $C_{18\text{-}3\text{-}1}$ is low and up to 40 wt%, the SAXS patterns show the characteristic of a micellar solution, and could be fitted with the core-shell model for the micelles. As the concentration of $C_{18\text{-}3\text{-}1}$ increases, an intensity increase is observed for the peak with a q value around 0.1 $Å^{-1}$ that is caused by a structure factor. The d-spacing calculated from the q value of this structure factor peak decreases when the concentration increases. When the concentration reaches 40 wt%, the micelles are random close packed.

At 45 wt%, the diffraction pattern can be indexed to the $P6_3/mmc$ structure. While the concentration of $C_{18\text{-}3\text{-}1}$ in water is in the range of 50 to 60 wt%, the $Pm\bar{3}n$ structure is observed. When the concentration of $C_{18\text{-}3\text{-}1}$ increases above 60 wt%, the diffraction peaks of the micellar cubic phase are not well resolved. Based on a calculation of micellar properties in the HCP $P6_3/mmc$ structure and the $Pm\bar{3}n$ structure, a rational for the occurrence of the HCP can be suggested.

The close packing (HCP and/or CCP) structures that have been observed, for instance, the HCP in the cationic alkyltrimethylammonium surfactant – water system with strongly hydrated counterions,[38] and the CCP in the $C_{12}EO_{12}$ – water system,[21] have been described as close packing of spherical aggregates. These structures are generally found in systems where the surfactant has a large head group, or where the surfactant is associated to strongly hydrated counterions. In both cases the micellar shell will contain a substantial amount of water. For comparison, in our system with the divalent head group, the micelles will not elongate and, further, the micellar shell contains 73 vol% of water (Paper I). Such micelles with a lot of water in the micellar shell, will be easily deformable, and would have the possibility to interact via faces instead of points. This would cause spherical micelles to form a more polyhedral like shape. The point group symmetry of this polyhedral like micelle may direct the packing of the third close packed layer, i.e. ABA or ABC, hence determining whether the structure is HCP or CCP. The $Pm\bar{3}n$ structure is explained by 2 of the 8 micelles in the unit cell retaining the same size as in the $P6_3/mmc$ structure while 6 of the 8 micelles adopt a larger size. The respective micelles have dodecahedral and 14-hedral shapes and thereby fill space.

5.1.2 $C_{18\text{-}3\text{-}1}$ surfactant in sodium chloride solutions

The CMC of $C_{18\text{-}3\text{-}1}$ is expected to decrease as the concentration of salt increases. The concentration of $C_{18\text{-}3\text{-}1}$ is selected to 0.025 mol/L as it is the concentration used in synthesis of the silica materials. The concentration is well above the CMC.

With an increase in the ionic strength of the solution, the micellar size does not change to any significant degree. The value of the effective hydrodynamic radius obtained by DLS (Figure 5.2, left) under concentrated salt conditions is in good agreement with the overall radius obtained by SAXS (Figure 5.2, right). The micellar size of the surfactant aggregates is around 6.5 nm in diameter.

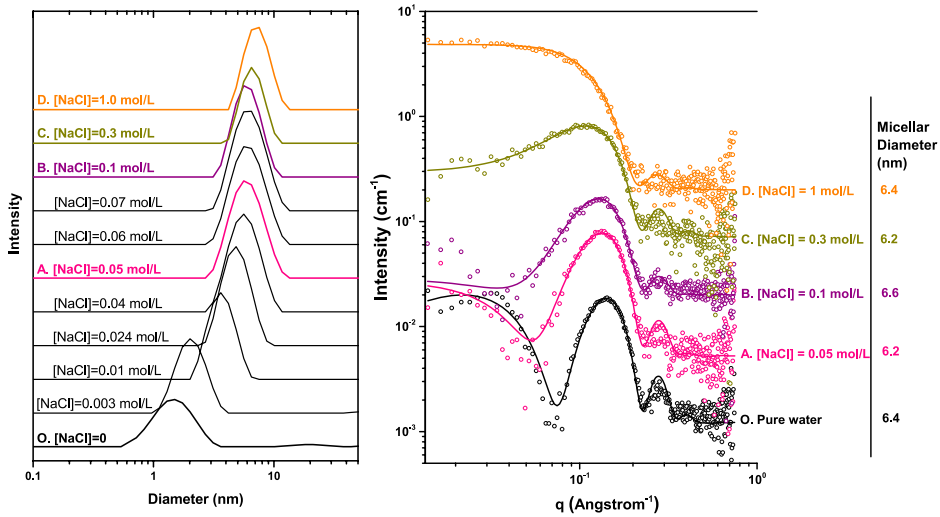

Figure 5.2. Dynamic Light Scattering (DLS) results (left) and SAXS patterns (right) of the micellar architectures of $C_{18\text{-}3\text{-}1}$ in different solutions. Sodium cloride was added in the $C_{18\text{-}3\text{-}1}$ solution with the concentration of 0.025 mol/L. Among the plots are (O) pure water, (A) [NaCl] = 0.05 mol/L, (B) [NaCl] = 0.1 mol/L, (C) [NaCl] = 0.3 mol/L and (D) [NaCl] = 1 mol/L. Right: the SAXS data (circles) are in absolute scale. The fittings were done using SasView (solid curves). The core-shell form factor and the Hayter structure factor are introduced to fit the data. The curves are shifted in y-axis, but kept in the same scale. The ticks on the y-axis are with respect to curve O.

The collective diffusion coefficient (D_c) measured by DLS is significantly dependent on interactions.[103] D_c is approximately related to $1/S(0)$, where $S(0)$ is the structure factor value at q=0 and proportional to the effective osmotic compressibility. In pure water there is a strong electrostatic repulsion between the micelles and $S(0) < 1$. With increasing salt concentration, this interaction is screened and $S(0)$ approaches 1, and the collective diffusion coefficient can be used to evaluate the micellar size (Figure 5.2, left). The changes observed in the SAXS patterns (Figure 5.2, right) are mainly an effect of changes in contrast caused by the presence of NaCl. In addition, it was found that the micellar size reached a similar size regardless of the type of ions present, when the ionic strength of the solution was above 0.12 mol/L.

These results indicate that addition of NaCl in the synthesis does not change the micellar size as the synthesis solution originally has a very high ionic strength. Furthermore, the presence of carboxylic entities will not lead to any drastic changes in the micellar size. We thus expect that micelles are robust and retain their size under all the synthesis conditions used in this system. All structures should hence be formed around the same initial structure directing aggregates.

5.2 Kinetic influence of siliceous reactions

The structural transformation from $Fm\bar{3}m$ to $Fd\bar{3}m$ in this synthesis system has been suggested to occur as an influence of the strength of the electrostatic interaction between the surfactant head group and the carboxylic group of the CSDA depending on pH, as a consequence of the varying ionization degree of the CSDA.[68, 70] However, our studies show that the pH dependence of the hydrolysis rate of TEOS is the origin of the structural change between $Fm\bar{3}m$ and $Fd\bar{3}m$, rather than the previously suggested ionization degree mechanism.[68, 70] This kinetic effect is generally overlooked in mechanistic discussions.

As stated in Chapter 2, the rate of the TEOS reactions (*i.e.* the hydrolysis and subsequent silica polymerization) varies to a great extent with the pH.[30, 32] The hydrolysis rate of TEOS reaches a minimum at a pH around 7, where the $Fd\bar{3}m$ structure is formed. Hence, the effects of the kinetics of the hydrolysis on the structural transformation between the $Fm\bar{3}m$ structure and the $Fd\bar{3}m$ structure have been investigated.

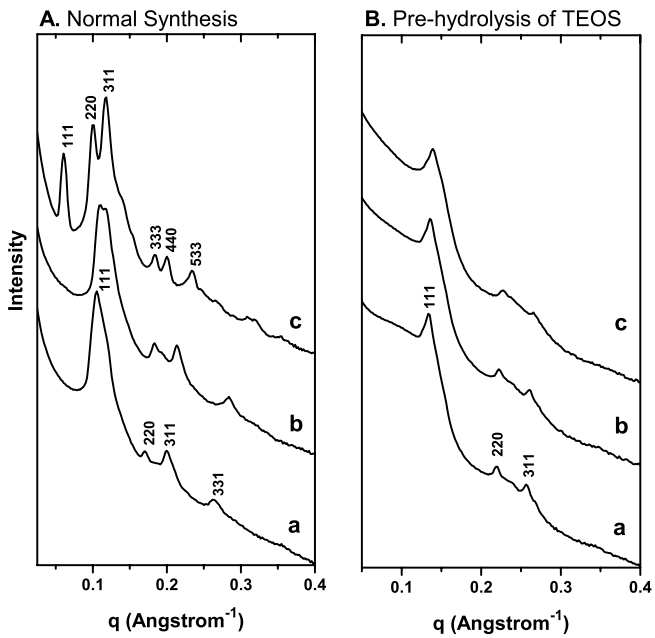

Figure 5.3. SAXD patterns of as-synthesized carboxylic group functionalized MSMs, synthesized at different pH, a) pH=9, b) pH=8, c) pH=6, and using, A) normal synthesis, and B) with pre-hydrolysis of TEOS. The chemical molar composition of the reaction mixture was $C_{18\text{-}3\text{-}1}$: 2CSDA: xHCl: 15TEOS: 2000H2O, a) x=1.4, b) x=1.6, c) x=1.8. The SAXD patterns are indexed with the $Fm\bar{3}m$ space group (A-a and B-a) and the $Fd\bar{3}m$ space group (A-c).

As the SAXD patterns show in Figure 5.3, in a normal synthesis (Fig. 5.3–A), at three different pH values the $Fm\bar{3}m$ (curve a), $Fd\bar{3}m$ (curve c) or an intergrowth of these structures (curve b) are produced. When the influence of TEOS hydrolysis is removed by hydrolyzing the TEOS prior to addition to the synthesis (Fig. 5.3–B), materials with $Fm\bar{3}m$ structure are formed regardless of the pH of the solution. Therefore, the $Fd\bar{3}m$ structure has a slower formation process than the $Fm\bar{3}m$ structure. Possibly formation of $Fm\,\bar{3}\,m$ relies on a system that arrives at a dynamical arrest induced by silica condensation.

Solid-state ^{29}Si NMR was used on as-synthesized materials to investigate if the kinetics of TEOS hydrolysis was reflected in the extent of cross-linking of silica.

Products from four syntheses were investigated. They were under conditions producing the $Fm\bar{3}m$ structure, at pH 9, and the $Fd\bar{3}m$ structure, at pH 6, as well as the corresponding conditions with the pre-hydrolysis step, i.e. producing the $Fm\bar{3}m$ structure in both cases. Peaks from ^{29}Si NMR spectra were fitted and integrated as described in the experimental section and the resulting values are shown in Table 5.1. Based on Q^3/Q^4, the extent of condensation of the two structures from normal syntheses is comparable. Moreover, $Q_{(sum)}$ represents the entire amount of silica originating from TEOS, and $T_{(sum)}$ is the amount originating from CSDA. In the $Fm\bar{3}m$ structure, the ratio of $T_{(sum)}/Q_{(sum)}$ is 0.11, while for the $Fd\bar{3}m$ structure, this ratio is slightly larger, i.e. 0.13. This suggests that formation of the $Fd\bar{3}m$ structure is characterized by more CSDA than does the $Fm\bar{3}m$ structure. The molar ratio of CSDA to TEOS in the synthesis mixture is 0.13, demonstrating that both structures require a large uptake of CSDA. The T^2 to T^3 ratio in the $Fd\bar{3}m$ structure is higher than in the $Fm\bar{3}m$ structure, suggesting that the CSDA in the $Fd\bar{3}m$ structure is less cross-linked.

Table 5.1. Silica cross-linking values based on solid-state ^{29}Si NMR results. Q refers to the silica and T to the CSDA.

Synthesis method	Synthesis pH	Structure	Q^4	Q^3	T^3	T^2	Q^3/Q^4	T^2/T^3	$T_{(sum)}/Q_{(sum)}$
Normal Synthesis	9	$Fm\bar{3}m$	0.53	0.36	0.08	0.02	0.68	0.25	0.11
	6	$Fd\bar{3}m$	0.50	0.33	0.07	0.04	0.66	0.57	0.13
Pre-hydrolysis of TEOS	9	$Fm\bar{3}m$	0.52	0.39	0.08	0.02	0.75	0.25	0.11
	6	$Fm\bar{3}m$	0.61	0.29	0.08	0.02	0.48	0.25	0.11

5.3 Influence of salt in the syntheses

In order to observe the effect of the strength of the electrostatic interaction, NaCl (from 0 to 2 mol/L) was added to syntheses performed at specific acid concentrations. These acid concentrations were chosen based on where the different structures were obtained as a function of the amount of added HCl, as shown in Chapter 3. Figure 5.4 shows a diagram of the structures obtained depending on concentration of NaCl and the pH measured after completed synthesis.

The bottom row in Figure 5.4, corresponding to no salt addition, represents the original structures as expected. A low concentration of NaCl, less than 0.05 mol/L, does not influence the structure formation – the same structures are obtained as when no NaCl was added. At a very high concentration of NaCl, above 0.5 mol/L, no well-defined structures were obtained.

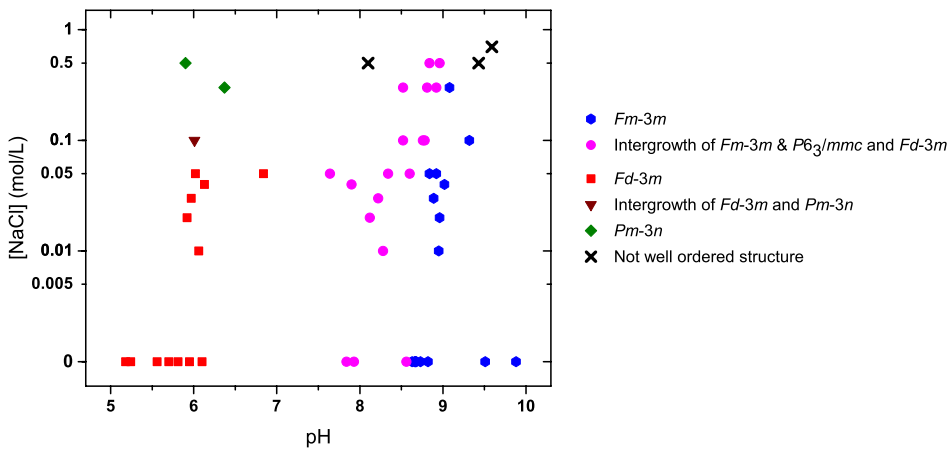

Figure 5.4. Structure Diagram of the synthesis system; concentration of NaCl vs. pH.

At high pH (above 9), a series was done using the synthesis system without HCl, which typically result in the $Fm\bar{3}m$ structure. The resulting SAXD patterns of the as-synthesized materials are shown in Figure 5.5, A. When the concentration of NaCl is below 0.5 mol/L, the structure is clearly resolved as the $Fm\bar{3}m$ structure from the SAXD data. At higher NaCl concentrations, even though the synthesis did not result in well-defined structures, the materials are probably still based on the $Fm\bar{3}m$ structure, as some of the broad peaks remain in the expected position range. Therefore the formation under these conditions is quite resilient to changes in the ionic strength – the driving force to

form the $Fm\bar{3}m$ structure is substantial. Only at very high ionic strength, i.e. at 2 mol/L NaCl, does the SAXD pattern lack observable peaks or shoulders.

At pH 6 the normal synthesis results in the $Fd\bar{3}m$ structure, but when the concentration of NaCl was between 0.3 mol/L and 0.5 mol/L, the $Pm\bar{3}n$ structure was obtained. The SAXD patterns of the resulting structures formed at pH 6, with increasing amount of salt, are shown in Figure 5.5, B. Hence addition of NaCl at low pH drives the structure towards the $Pm\bar{3}n$ structure.

As discussed above, the kinetics of the system is responsible for the structural variation with pH. From the results of Figure 5.4 the influence of the kinetics is still apparent. A synthesis relying on fast kinetics (pH above 8) is generally not greatly influenced by the ionic strength (Figure 5.5, A). The same structure is obtained regardless of the amount of salt added. On the other hand, when the dynamics of the system is slow a structural transition from the $Fd\bar{3}m$ structure to the $Pm\bar{3}n$ structure, is observed with increasing ionic strength (Figure 5.5, B).

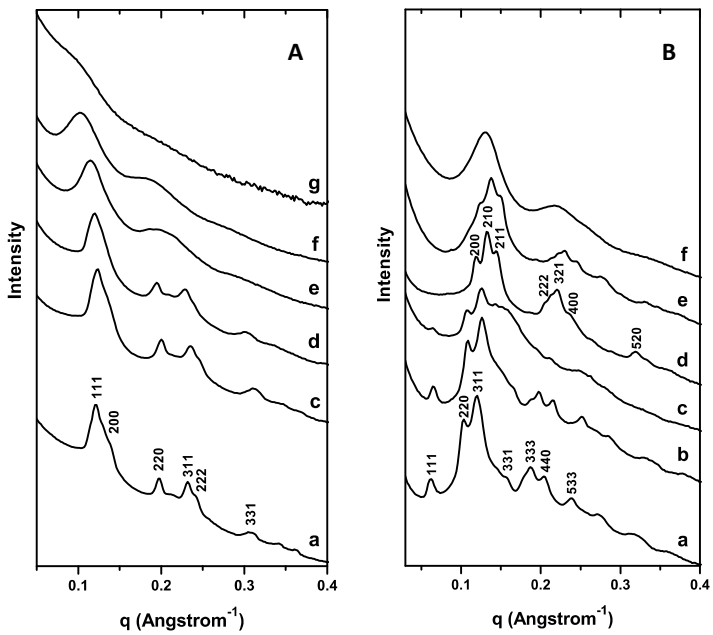

Figure 5.5. SAXD patterns of carboxylic group functionalized MSMs under high pH (above 9) conditions without addition of HCl (A), and under pH=6 conditions with 0.0425 mol/L of HCl (B), with addition of NaCl. The chemical molar composition of the reaction mixture was $C_{18\text{-}3\text{-}1}$: 2CSDA: 0 (or 1.7) HCl: 15TEOS: 2000H_2O: x NaCl, (a) [NaCl] = 0 (x=0), (b) [NaCl] = 0.05 mol/L (x=2), (c) [NaCl] = 0.1 mol/L (x=4), (d) [NaCl] = 0.3 mol/L (x=12), (e) [NaCl] = 0.5 mol/L (x=20), (f) [NaCl] = 1.0 mol/L (x=40), and (g) [NaCl] = 2.0 mol/L (x=80). Curve left–a is indexed with the $Fm\bar{3}m$ structure, curve right–a is indexed with the $Fd\bar{3}m$ structure, and curve right–d is indexed with the $Pm\bar{3}n$ structure.

Syntheses under conditions that form the $Fd\bar{3}m$ structure and the $Pm\bar{3}n$ structure were also performed with investigation of the effect of kinetics of TEOS hydrolysis, as introduced previously. The results show the same phenomenon that materials formed when TEOS was pre-hydrolyzed can be indexed with the $Fm\bar{3}m$ space group, whereas when a large amount of NaCl is added the structure becomes less defined. From the discussion above combined with the pre-hydrolysis results, the formation of the $Pm\bar{3}n$ structure requires even slower kinetics of the TEOS reactions, which can be achieved at high concentration of NaCl.

5.4 Insight into the formation of $Fm\bar{3}m$, $Fd\bar{3}m$ and $Pm\bar{3}n$ structures

In an effort to have a deep insight into the synthesis processes that form different structures, ^{13}C PT ssNMR and SAXD measurements were used to investigate the as-synthesized samples at different synthesis stages: after 2 hours of reaction and after 2 days of hydrothermal treatment. In addition, as results in the $Fd\bar{3}m$ and $Pm\bar{3}n$ structures were significantly different at these points in time, these structures were also investigated in the interim window, after 1.5 and 7 hours of hydrothermal treatment, respectively.

As mentioned in Chapter 4, among the PT ssNMR measurements, the CP and INEPT signals provide information about the rigidity and mobility coupled with the isotropic and anisotropic C-H bond reorientation. Information for each segment of the molecules can be explored.

As shown in Figure 5.6, it is clear that the $Fm\bar{3}m$, $Fd\bar{3}m$ and $Pm\bar{3}n$ structures give rise to very different CP and INEPT signals after 2 hours of synthesis (spectra a). In the $Fm\bar{3}m$ structure, the spectra were dominated by a CP signal, except for a few segments in the chain. This indicates that the head group and the carbon chain are quite rigid and show anisotropic behavior. On the other hand, in the $Fd\bar{3}m$ and the $Pm\bar{3}n$ structures, all segments in the surfactant and the CSDA have very high INEPT intensity and almost no CP signal, which corresponds to fast and isotropic mobile behavior. However, for the $Pm\bar{3}n$ structure, the methylene group (IV) and the methyl groups (V) in TEOS and/or ethanol shows a CP signal. As both ethanol molecules and TEOS monomers should show a fast and isotropic behavior, this CP signal is somewhat surprising. Possibly it arises from large silica oligomers that are not fully hydrolysed and, as a consequence of the high concentration of Na^+ present,[31] which was discussed in Chapter 2. Such aggregates are expected to have slower mobility than ethanol or TEOS molecules and would hence give rise to a stronger CP signal. This signal later disappears, possibly as a consequence of continued hydrolysis.

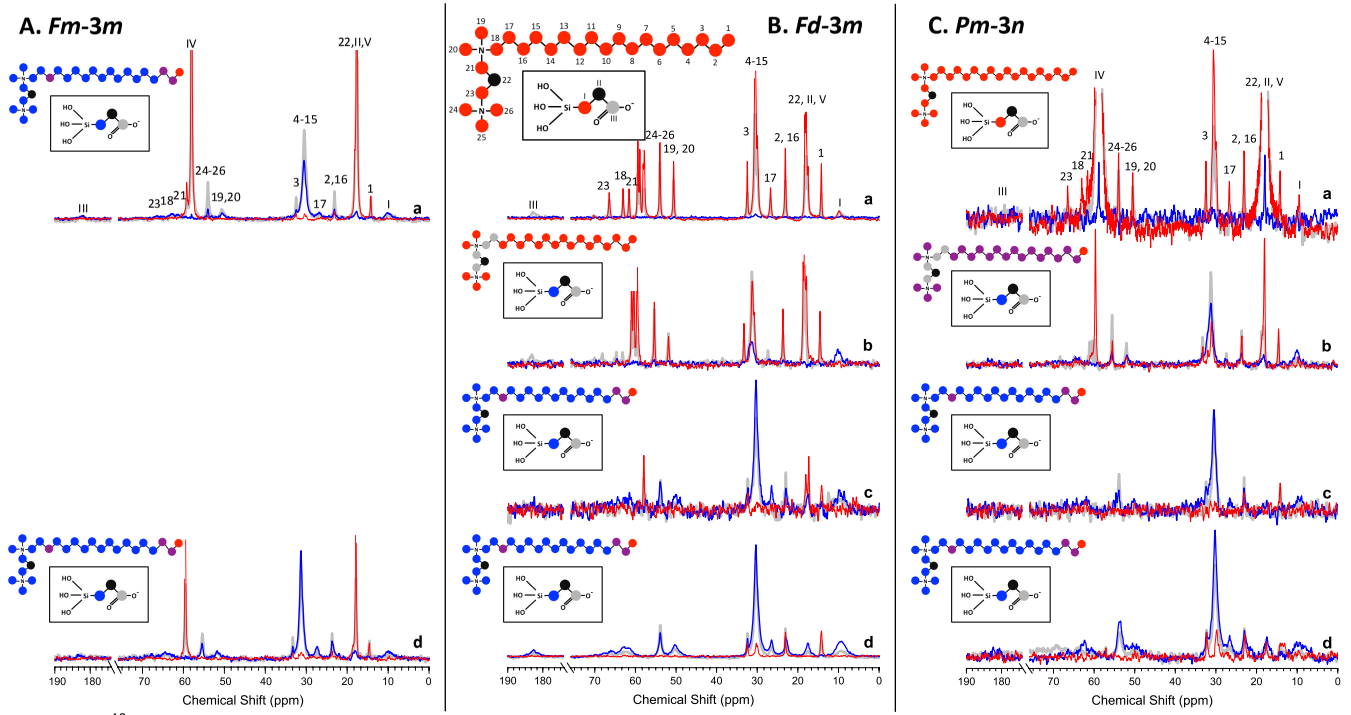

Figure 5.6. ^{13}C MAS NMR spectra (DP - grey, CP - blue, and INEPT - red) of (A) $Fm\bar{3}m$, (B) $Fd\bar{3}m$ and (C) $Pm\bar{3}n$, at different stages of synthesis, (a) after two hours of synthesis (before hydrothermal treatment), (b) after 1.5 hours of hydrothermal treatment, (c) after 7 hours of hydrothermal treatment, and (d) dry sample after 48 h hydrothermal treatment The chemical molar composition of the reaction mixture was $C_{18\text{-}3\text{-}1}$: 2CSDA: xHCl: 15TEOS: yNaCl: 2000H_2O, (A) x=1.4, y=0, (B) x=1.7, y=0, (C) x=1.7, y=12. The chemical structures of the surfactant and the CSDA are depicted with respect to the different mobility of the carbon segments, illustrated as circles. The segments are numbered with Arabic numbers (1-26) in the surfactant molecule and with Roman numerals in the CSDA (I-III). The methylene and methyl groups, in ethanol or TEOS, are numbered IV and V respectively. The colors of the circles illustrate the dynamics and anisotropy: fast isotropic (red), fast anisotropic (purple), rigid (blue), and slow motion with τ_c between 0.1 and 10 us (grey). Black circles are used for segments that cannot be distinguished due to overlap, such as 22, II, and V. The intensities in the same set of DP-CP-INEPT experiments were normalized against the DP intensity of the –CH3 group in the tail (1). All spectra are plotted at the same scale.

After 1.5 hours of hydrothermal treatment, in both the $Fd\bar{3}m$ and $Pm\bar{3}n$ structures, the $-CH_2$ groups (17, 18, 21, 23), close to the nitrogen in the surfactant, only give rise to a DP signal, signifying that they are in very slow movement (correlation time between 0.1-10 μs). The segment I in the CSDA shows only a CP signal, which means that the CSDA is fixed. In the $Fd\bar{3}m$ structure, all the other segments in the surfactant have a high INEPT signal (correlation time < 0.1 μs). In the $Pm\bar{3}n$ structure on the other hand, the $-CH_3$ in the head group and the $-CH_2$ in the carbon chain show similar intensity for both CP and INEPT, indicating that these segments have a fast but anisotropic behavior. In brief, at 1.5 hours of hydrothermal treatment, the CSDA is fixed in both structures: in the $Fd\bar{3}m$ structure, the surfactant head group starts to become fixed, while in the $Pm\bar{3}n$ structure, the surfactant is more fixed than in the $Fd\bar{3}m$ structure.

From 7 hours of hydrothermal treatment until the synthesis is complete after 2 days, the products of the three structures give rise to similar NMR spectra. The CSDA is fixed. The carbons in the surfactant are mostly rigid, except for the ones in the surfactant's very tail. This confirms that all these three structures are fixed.

In addition, the synthesis process of the $Fm\bar{3}m$, $Fd\bar{3}m$ and $Pm\bar{3}n$ structures was also followed by SAXD (Figure 5.7), complementary to the ^{13}C PT ssNMR measurements. These SAXD patterns, in Figure 5.7, yield structure information about the products depending on time. 2 hours into the reaction (a curves), the SAXD pattern of the $Fm\bar{3}m$ synthesis is dominated by peaks that correspond to this space group. However at this time, the $Fd\bar{3}m$ and $Pm\bar{3}n$ structures are not well developed and show similar SAXD patterns. The lattice spacing in the synthesis of the $Pm\bar{3}n$ structure is larger than in the synthesis of the $Fd\bar{3}m$ structure. After 1.5 h under hydrothermal treatment (b curves), both the $Fd\bar{3}m$ and $Pm\bar{3}n$ structures give rise to SAXD peaks consistent with the space groups corresponding to the final materials. However, the pattern for the $Pm\bar{3}n$ structure is not as well defined as the $Fd\bar{3}m$ structure at this time, and can be indexed by both the $Pm\bar{3}n$ and the $Fd\bar{3}m$ space groups. From 7 hours of hydrothermal treatment (c curves) until the synthesis is completed after 2 days (d curves), the peaks of the final structures clearly dominate the diffraction patterns, and with time, the lattice parameter decreases. The decrease is consistent with the expected silica condensation during the synthesis.

The NMR combined with the SAXD results is in agreement with the findings presented above; the $Fm\bar{3}m$ structure, formed at a pH where the kinetics of the silica condensation is fast, contains surfactant and CSDA that quickly get stuck in the structure (low INEPT signal already after 2 h), whereas the $Fd\bar{3}m$ structure and $Pm\bar{3}n$ structure, whose formations rely on slow condensation, contains surfactant and CSDA molecules that are still flexible after 2 hours of reaction. In addition, the $Pm\bar{3}n$ structure, formed in the presence of high concentration of NaCl, is synthesized through a slower process than the $Fd\bar{3}m$ structure. This was clear from the SAXD results (Figure 5.7). The NMR investigation (Figure 5.6), however, points in another direction. It is in the synthesis of the $Pm\bar{3}n$ structure that the surfactant becomes rigid earlier. This could be the result of

aggregation of silica oligomers that have not been fully hydrolyzed caused by aggregation induced by the presence of salt, not via covalent bonding. The SAXD result (Figure 5.7, curve C-b) indicates that $Fd\bar{3}m$ is a transient phase during the formation of $Pm\bar{3}n$. As the micelles are more or less of similar size, the changes in structures cannot be a consequence of difference in the micellar aggregates. Possibly the presence of salt promotes aggregation of silica species, which induces a flexibility of the system that allows the mesostructure to develop further.

Therefore these three main structures formed in this synthesis system are a result of the extent of rearrangement possible after the aggregation. The driving force for the system is to arrive at the densest structure possible, which could be a consequence of the smallest interface area. In this study, the structure gets denser in the order of $Fm\bar{3}m$, $Fd\bar{3}m$ to $Pm\bar{3}n$.

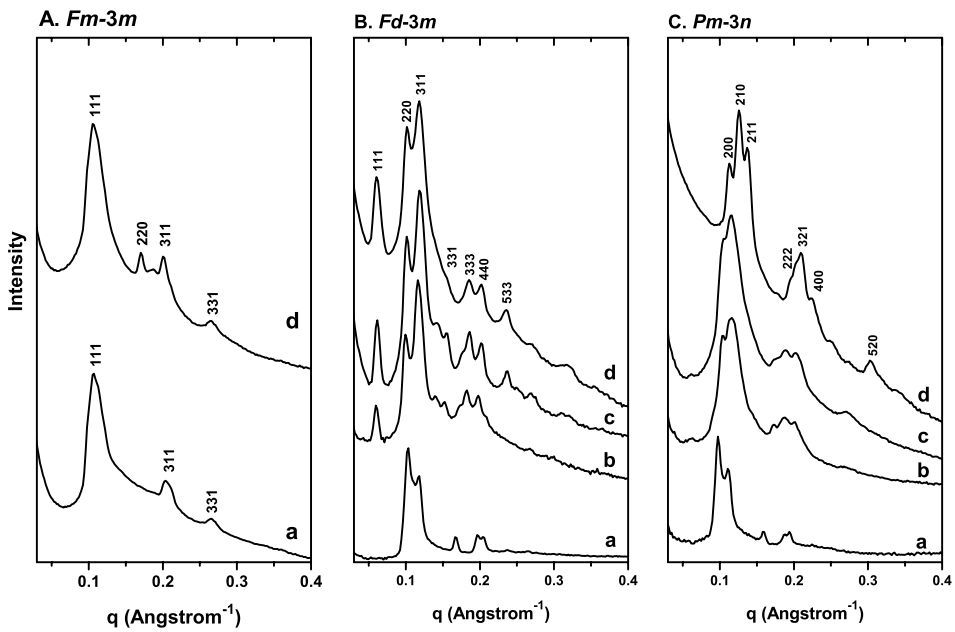

Figure 5.7. SAXD patterns of of (A) $Fm\bar{3}m$, (B) $Fd\bar{3}m$ and (C) $Pm\bar{3}n$, at different stages of synthesis: (a) after two hours of synthesis (before hydrothermal treatment), (b) after 1.5 hours of hydrothermal treatment, (c) after 7 hours of hydrothermal treatment, and (d) dry sample after 48 h hydrothermal treatment The chemical molar composition of the reaction mixture was $C_{18\text{-}3\text{-}1}$: 2CSDA: xHCl: 15TEOS: yNaCl: 2000H_2O, (A) x=1.4, y=0, (B) x=1.7, y=0, (C) x=1.7, y=12.

5.5 The role of CSDA

In order to observe the influence of only CSDA, different concentrations of CES were added in the typical synthesis without addition of HCl. The addition of CES results in a pH above 8.5. The molar ratio of CES/$C_{18\text{-}3\text{-}1}$ is varied from 0.1 to 2.

The resulting SAXD patterns of the as-synthesized materials are shown in Figure 5.8. The $Fm\bar{3}m$ structure is obtained when the molar ratio of CES/$C_{18\text{-}3\text{-}1}$ is above 0.75. The lattice parameter decreases as concentration of CES decreases. This phenomenon was also obtained by Han et al. when they controlled the CES/$C_{18\text{-}3\text{-}1}$ ratio higher than 2.[70] When the concentration of CES decreases with molar ratio CES/$C_{18\text{-}3\text{-}1}$ below 0.75, it has a big influence on the structure formation. For this divalent cationic surfactant, it needed at least a 0.3:1 ratio of CES to surfactant to form well-defined structures, and at least a 1:1 ratio to form the $Fm\bar{3}m$ structure.

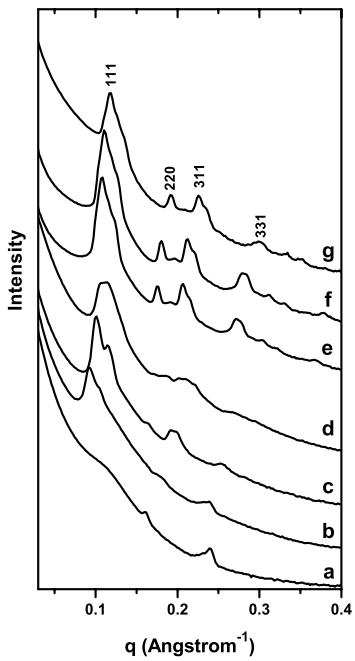

Figure 5.8. SAXD patterns of carboxylic group functionalized mesoporous silica materials with the final composition, $C_{18\text{-}3\text{-}1}$: xCSDA: 15TEOS: 2000H_2O, (a) x=0.1, (b) x=0.3, (c) x=0.5, (d) x=0.75, (e) x=1.0, (f) x=1.2, and (g) x=2.0.

CES in different concentrations was added to syntheses performed at specific acid concentrations. SAXD was done to the as-synthesized products of these syntheses. A structure diagram showing the composition of CES vs. pH based on the SAXD measurements was produced and is shown in Figure 5.9. As above, when CES/$C_{18\text{-}3\text{-}1}$ is higher than 1.0, this molar ratio does not influence the structure formation. It is the pH value of the synthesis solution that determines which structure is formed. As the pH increases above 4, the *Ia*$\bar{3}$*d* structure, the *Fd*$\bar{3}$*m* structure, the intergrowth structure of *Fd*$\bar{3}$*m* and *Fm*$\bar{3}$*m*, and the *Fm*$\bar{3}$*m* structure are formed, respectively.

This pH dependent structural transformation presents a similar trend as the structure diagram show in Figure 3.2, from the reversed system. Therefore, our investigation on the structural formation mechanism may apply in both of these reversed systems. It indicates that the structure formation of *Fm*$\bar{3}$*m* relies on fast kinetics of silica reactions. However, this requires a contribution of CSDA with molar ratio of CSDA/divalent surfactant higher than 1.0.

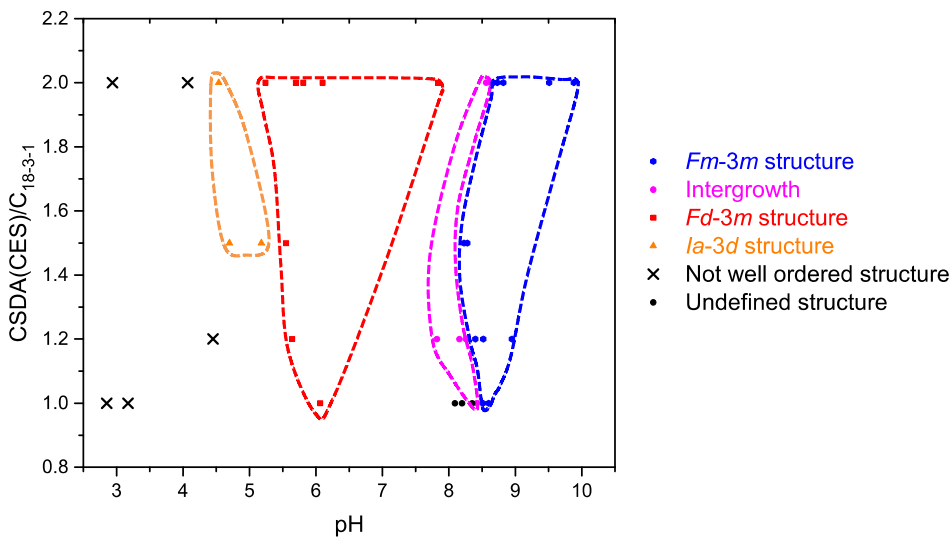

Figure 5.9. Structure Diagram of the synthesis system; composition of CES vs. pH; the molar composition is $C_{18\text{-}3\text{-}1}$: xCSDA: yHCl: 15TEOS: 2000H_2O (x=1–2, y=0–3.2).

6 System 2: synthesis of chiral mesoporous silicas

Cryo-TEM and cryo-SEM were used to investigate the formation processes of helical ribbons of MSMs synthesized under 0˚C using C_{14}-L-Ala as structure directing agent, APES as CSDA, and TEOS as silica source. Since the cryogenic electron microscopies allow us to have an obvious view of things happening in the synthesis solution, for this study, the aim is to have a deep insight into the formation process of the helical ribbons. The results presented here include the principal results reported in paper V.

Cryo-TEM and cryo-SEM measurements were done in parallel for the synthesis solution at different reaction times. Time 0 is defined as the time when TEOS and CSDA are added. The cryo-TEM measurements provide interesting information on several different objects/morphologies. As shown in Figure 6.1, the images show the presence of spherical particles, fibers, twisted ribbons, helical ribbons, tubes and species without distinct morphology (amorphous aggregate) as well as ethane contamination. Some of these morphologies appear or disappear with time, while others are always present but with different characteristics. The cryo-SEM images do not provide reliable information during the early synthesis stages. However, after 30 min, the ribbons and tubes are obvious. The presence of these morphologies agrees very well with the corresponding cryo-TEM images.

Fiber morphologies were detected from 3 min to 15 min. The widths of the fibers increase with time. When the widths of the fibers are above 14 nm, they become twisted ribbons. From 3 min to 10 min, the ribbons are mainly twisted, while from 23 min, mainly helical ribbons were obtained. This is in accordance with the suggestion that ribbons go from twisted to helical form as the width increases.[74] The widths and pitches of the ribbons increase as a function of time. Furthermore, tubes can be observed after 27 min. In short, the ribbons twist, and with time grow in width, eventually forming helical ribbons, and later merge into tubes (see Figure 6.2).

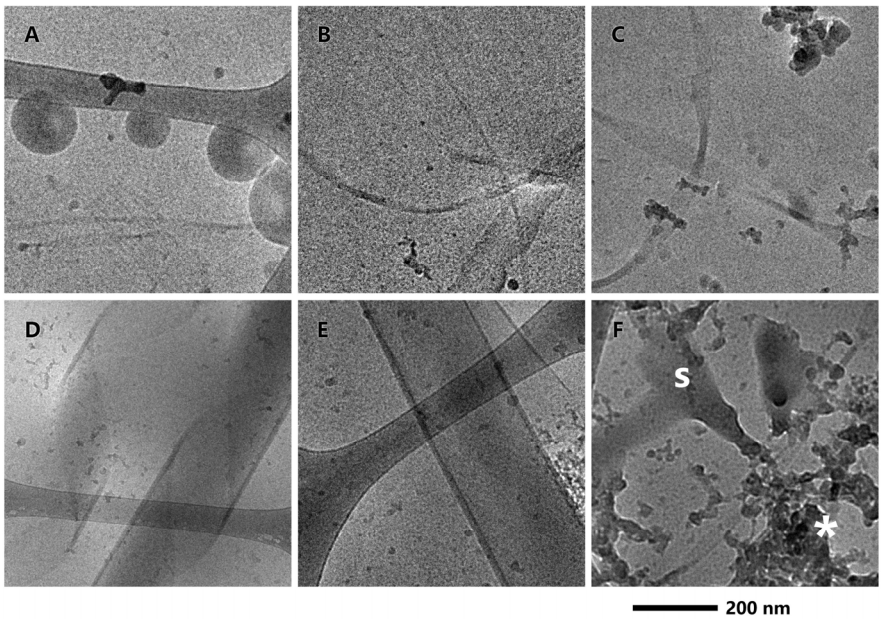

Figure 6.1. cryo-TEM images with different morphologies investigated in the helical ribbon synthesis process. (A) spherical particles, (B) fibers, (C) twisted ribbons, (D) helical ribbons, (E) tubes, (F) species without distinct morphology (marked with a "s") and ethane contamination (marked with a "*").

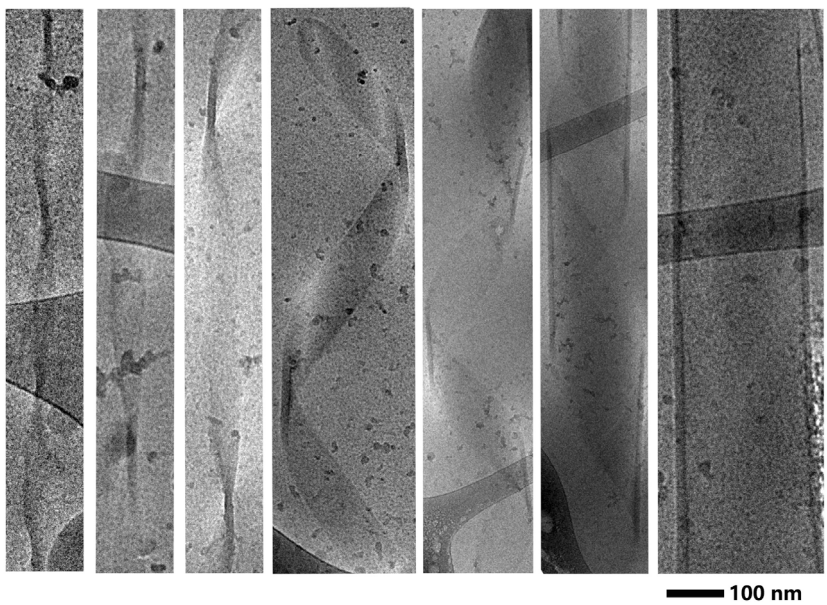

Figure 6.2. cryo-TEM images with twisted ribbons and helical ribbons.

A geometric-mechanical model has been reported by Sharon *et al.* to explain the mechanism of the configuration evolutionary process of helical ribbons. It was first used to study the mechanical process of seedpods opening into chiral structures, i.e. from flat to helix. The theory is based on a mathematical framework of "incompatible elasticity". The pod can be modelled as a thin strip with a flat intrinsic metric and a saddle-like intrinsic curvature.[104] Obviously the bending of an initially flat strip into a saddle-like configuration cannot be achieved without stretching the sheet, which means that elastic energy is stored in the system. Hence the general mathematical framework is developed that the configuration of the strip is fully characterized by two two-dimensional tensors: a curvature tensor describing the local curvature of the sheet, and a metric tensor describing the distance between points on the surface of the strip. They then minimize the total elastic energy of the strip, that is, the sum of bending and stretching energy.[105]

$$E_{elastic} \approx t\left(K - K(\bar{a})\right)^2 lw^5 + t^3(b - \bar{b})^2 lw \qquad (6.1)$$

As shown in Figure 6.3, a quantitative study of strips cut out from latex sheets at an angle of $\theta = 45°$ exhibits two different regimes: wide strips adopt a configuration of cylindrical helices, whereas narrow strips exhibit as twisted helices, where the strip's centerline is straight.

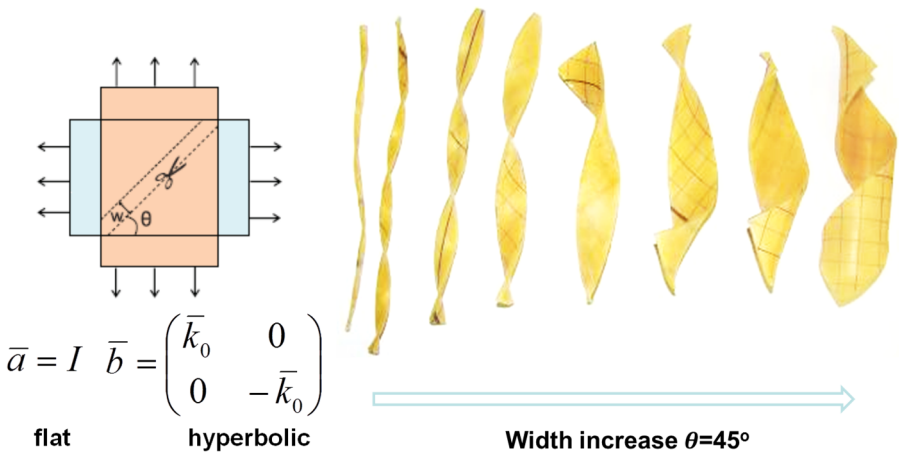

Figure 6.3. Two planar latex sheets are stretched uniaxially along perpendicular directions and then glued together, forming a residually stressed compound sheet. A strip is then cut from this sheet along a direction that forms an angle θ with one of the stretching directions. The configuration of the strips changes from twisted and helical as the width increases. They are cut from the latex sheets at angles θ = 45° (the grids are parallel to the directions of principal curvature).

At the coarsest level, the shape of the strips can be characterized by the radius (r) and the pitch of the strip's midcurve (p). Figure 6.4 shows the plot of the dimensionless pitch

$\tilde{p} = pk_0$ and the dimensionless radius $\tilde{r} = rk_0$ as functions of the dimensionless width $\tilde{w} = w\sqrt{k_0/t}$, where t is the thickness of the strip, and k_0 is estimated by measuring the curvature of very thin strips cut along principal directions. From the plot, there is a critical transition between the two regimes: cylindrical helices and twisted helices. Below the critical width, the radius $\tilde{r}$ is nearly 0, whereas it increases above the critical width and reaches a constant value as the width increases. The pitch $\tilde{p}$ attains a maximum at a value of about the critical width. The theoretical study consists of minimizing the energy (Eq. 1) of a strip with reference tensors $\bar{a}$ and $\bar{b}$ (as shown in Figure 6.3). The energy consists of the stretching energy and the bending energy. The stretching-dominated regime occurs with large w and the bending-dominated regime occurs with small w. The transition between the two regimes is expected to occur when the two energies are of comparable magnitude.

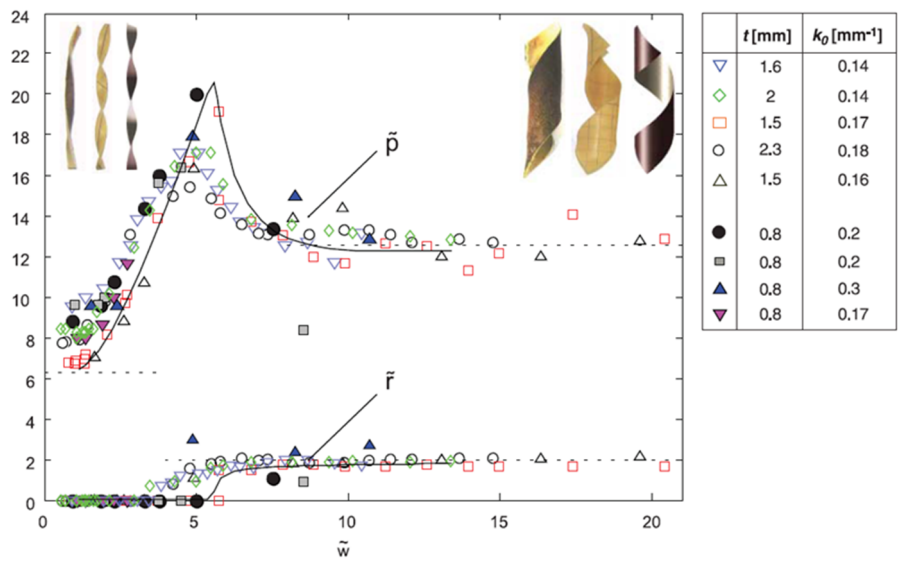

Figure 6.4. Dimensionless radius, $\tilde{r} = rk_0$, and pitch, $\tilde{p} = pk_0$, versus dimensionless width, $\tilde{w} = w\sqrt{k_0/t}$, for various strips cut from latex sheets at q = 45° (open symbols); different samples differ in k_0 and t (legend to right).The solid lines are the theoretical predictions, and the dotted lines are the asymptotic limiting values (Eq. 4). Insets show equilibrium configurations of (middle) latex strips along with (right) the theoretical prediction in both (left inset) narrow and (right inset) wide regimes. From ref. [104].*

* From Armon, S.; Efrati, E.; Kupferman, R.; Sharon, E., Geometry and Mechanics in the Opening of Chiral Seed Pods. Science 2011, 333, 1726-1730. Reprinted with permission from American Association for the Advancement of Science.

By measuring the width, pitch, and diameter of the ribbons obtained in this synthesis, a similar plot has been produced (see Figure 6.5). The curve is comparable to Figure 6.4, hence the characteristics of the twisted ribbons and helical ribbons are similar to the configurations of twisted helices and cylindrical helices observed in strips with a single intrinsic curvature. However, there is a fundamental difference between these two cases because in the case of a single curvature, the two tensors a and b are compatible and there is no mechanical frustration. In our case, a and b are incompatible, resulting in stored mechanical energy. Hence there is a configuration transformation based on time. Moreover, the ribbons are found to have 4 or 5 layers in the final products. The energy that is described in Sharon's theory could be an explanation for this phenomenon.

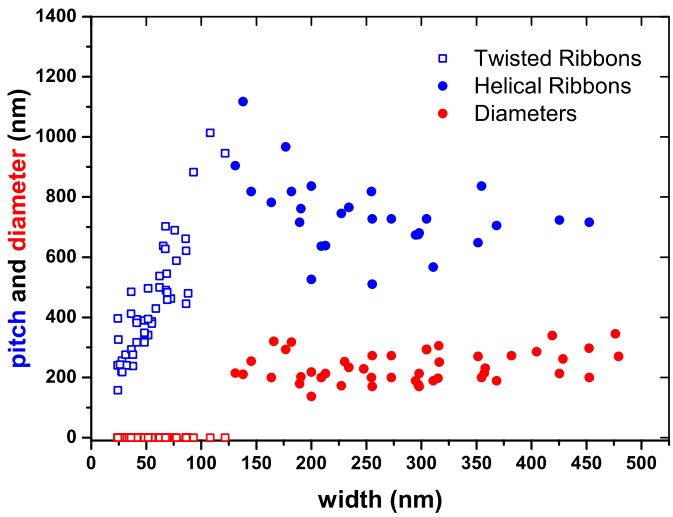

Figure 6.5. The samples synthesized at 0°C with different reaction times; the plot show measurements of diameter (in red) and pitch (in blue) as a function of width. The empty shapes represent the twisted ribbons, and the solid shapes are helical ribbons.

Furthermore, at the initial stages of the synthesis many spherical objects were present. They were detected from 3 min up to 23 min of reaction. At 27 min, some images showed "destroyed spheres". Additionally, almost all the spheres appeared in the vicinity of the carbon film, which indicate that the spheres are hydrophobic. At 0°C, TEOS hydrolysis and condensation are slow. It is possible that at the early stage of the synthesis, after TEOS is added, it is predominantly present as oil droplets, or spheres. Possibly the "destroyed spheres" are remnants of these, caught just when the hydrolysis is done.

7 Summary and Outlook

In this thesis work, detailed investigations of the formation of mesoporous silicas following the CSDA approach, from the starting solution to final product, have been performed for two synthesis systems: System 1) Synthesis of carboxylic group functionalized MSMs using $C_{18\text{-}3\text{-}1}$ as structure directing agent and CES as CSDA; and System 2) Synthesis of chiral MSMs with helical ribbon morphology.

In System 1, the investigation was focused on four interrelated parts. (1) $C_{18\text{-}3\text{-}1}$ in pure water has a CMC of 1.5 mmol/L. Self-assembly of $C_{18\text{-}3\text{-}1}$ forms two types of liquid-crystalline micellar phases, $P6_3/mmc$ and $Pm\bar{3}n$. The HCP structure is suggested to be due to the micelles being non-spherical and carrying a symmetry that dictates the $P6_3/mmc$ phase. At a concentration of 0.025 mol/L, the same as in the synthesis of MSM, the micellar size of $C_{18\text{-}3\text{-}1}$ is independent of the concentration of salt, which indicates the same micellar size in the formations of different structures. (2) The pH dependence of the hydrolysis rate of TEOS is the origin of the structural change between $Fm\bar{3}m$ and $Fd\bar{3}m$. Both the $Fm\bar{3}m$ and the $Fd\bar{3}m$ structures have a similar extent of cross-linking of silica, and for the formation of the $Fd\bar{3}m$ structure, the cross-linking of CSDA is lower than that of the $Fm\bar{3}m$ structure. (3) Salt plays a role by screening the charges, increasing the lattice parameter, as well as influencing the aggregation of silica oligomers. At high pH, when the kinetics of silica reaction is fast, a large amount of salt (0.5 mol/L) is required in order to influence the structure formation. At low pH, where the formation of the $Fd\bar{3}m$ structure relies on the slow kinetics of the reactions of the silica source, with presence of salt (0.3 mol/L), the $Pm\bar{3}n$ structure is obtained. (4) A CSDA/$C_{18\text{-}3\text{-}1}$ molar ratio of at least 0.5 is required to synthesize well-defined MSMs. The structural diagram that results from varying the $C_{18\text{-}3\text{-}1}$-HCl-CES composition ratios is comparable to the synthesis-field diagram of the reversed system, using C_{14}Glu, NaOH and TMAPS. As a short-term outlook for System 1, some the materials synthesized for the synthesis-field diagram need to be identified. Moreover, a *p6mm* structure is expected to exist in this system.

PT ssNMR and SAXD (ex-situ) measurements give an insight into the synthesis process of the $Fm\bar{3}m$, $Fd\bar{3}m$ and $Pm\bar{3}n$ structures that are formed in this system. The

$Fm\bar{3}m$ structure is a result of fast kinetics, while the $Fd\bar{3}m$ and $Pm\bar{3}n$ structures rely on slow processes, and between them, the $Pm\bar{3}n$ structure process is slower. The structure formed in this synthesis system is a result of the extent of rearrangement possible after the aggregation. The structure gets denser in the order $Fm\bar{3}m < Fd\bar{3}m < Pm\bar{3}n$. The driving force for the system is to arrive at the densest structure possible.

In System 2, the cryo-TEM and cryo-SEM images provide detailed information about the formation process of the synthesis. A formation mechanism could be suggested. First, the formation is possibly dependent on the slow hydrolysis rate of TEOS. The initial objects observed are fibers, twisted ribbons, helical ribbons and tubes. The fibers grow in width, or alternatively assemble into ribbons. They mainly appear at an early synthesis stage. With time the twisted ribbons grow in width and pitch. From 23 min, mainly helical ribbons were obtained. The twisted ribbons eventually form helical ribbons. Some of them later on merge into tubes. The evolution of the configurations could be explained by the incompatible elastic sheet theory. Further work is needed to complete this model, which accounts for a wider range of intrinsic geometries, and to collect digital information and describe configurations of chiral materials that are currently not well understood.

The CSDA method is a versatile way to synthesize MSMs with novel structures and diverse properties. This one-pot synthesis of functionalized MSMs also has good prospects for different applications. Especially, the chiral mesoporous materials are expected to make important contributions in life science. A deep understanding of the mechanism using the CSDA approach will open up the route to a more precise control of the structure, morphology, and properties of the mesoporous materials. Hence, a "cookbook" for directing the synthesis using the CSDA method will be very useful not only in designing novel surfactants and CSDAs that produce MSMs with unique characteristics, but also for synthesizing useful MSMs using environmentally friendly and inexpensive compounds. On the other hand, in order to draw firm conclusions regarding general mechanism of the CSDA route, a larger range of systems has to be investigated in detail.

References

1. Rouquerol, J.; Avnir, D.; Fairbridge, C. W.; Everett, D. H.; Haynes, J. H.; Pernicone, N.; Ramsay, J. D. F.; Sing, K. S. W.; Unger, K. K., Recommendations for the Characterization of Porous Solids. *Pure Appl. Chem.* **1994**, *66*, 1739-1758.
2. Breck, D. W., *Zeolite Molecular Sieves: Structure, Chemistry, and Use*; Wiley: Wiley-Interscience Publication, 1973.
3. Baerlocher, C.; McCusker, L. B.; Olson, D. H., *Atlas of Zeolite Framework Types*, 6 ed.; Elsevier Science: The Netherlands 2007.
4. Davis, M. E., Zeolites from a Materials Chemistry Perspective. *Chem. Mater.* **2014**, *26*, 239-245.
5. Sanders, J. V., Colour of Precious Opal. *Nature* **1964**, *204*, 1151-&.
6. Sanders, J. V., Diffraction of Light by Opals. *Acta Crystallographica Section a-Crystal Physics Diffraction Theoretical and General Crystallography* **1968**, *A 24*, 427-&.
7. Mayoral, R.; Requena, J.; Moya, J. S.; Lopez, C.; Cintas, A.; Miguez, H.; Meseguer, F.; Vazquez, L.; Holgado, M.; Blanco, A., 3d Long-Range Ordering in an Sio2 Submicrometer-Sphere Sintered Superstructure. *Adv. Mater.* **1997**, *9*, 257-&.
8. Stein, A.; Schroden, R. C., Colloidal Crystal Templating of Three-Dimensionally Ordered Macroporous Solids: Materials for Photonics and Beyond. *Current Opinion in Solid State & Materials Science* **2001**, *5*, 553-564.
9. Fudouzi, H.; Xia, Y. N., Colloidal Crystals with Tunable Colors and Their Use as Photonic Papers. *Langmuir* **2003**, *19*, 9653-9660.
10. Kloprogge, J. T., Synthesis of Smectites and Porous Pillared Clay Catalysts: A Review. *J. Porous Mater.* **1998**, *5*, 5-41.
11. Yanagisawa, T.; Shimizu, T.; Kuroda, K.; Kato, C., The Preparation of Alkyltrimethylammonium-Kanemite Complexes and Their Conversion to Microporous Materials. *Bull. Chem. Soc. Jpn.* **1990**, *63*, 988-992.
12. Beck, J. S., et al., A New Family of Mesoporous Molecular-Sieves Prepared with Liquid-Crystal Templates. *J. Am. Chem. Soc.* **1992**, *114*, 10834-10843.
13. Kresge, C. T.; Leonowicz, M. E.; Roth, W. J.; Vartuli, J. C.; Beck, J. S., Ordered Mesoporous Molecular-Sieves Synthesized by a Liquid-Crystal Template Mechanism. *Nature* **1992**, *359*, 710-712.

14. Vartuli, J. C.; Kresge, C. T.; Leonowicz, M. E.; Chu, A. S.; McCullen, S. B.; Johnsen, I. D.; Sheppard, E. W., Synthesis of Mesoporous Materials - Liquid-Crystal Templating Versus Intercalation of Layered Silicates. *Chem. Mater.* **1994**, *6*, 2070-2077.
15. Vartuli, J. C., et al., Effect of Surfactant Silica Molar Ratios on the Formation of Mesoporous Molecular-Sieves - Inorganic Mimicry of Surfactant Liquid-Crystal Phases and Mechanistic Implications. *Chem. Mater.* **1994**, *6*, 2317-2326.
16. Kresge, C. T.; Roth, W. J., The Discovery of Mesoporous Molecular Sieves from the Twenty Year Perspective. *Chem. Soc. Rev.* **2013**, *42*, 3663-3670.
17. Huo, Q. S., et al., Organization of Organic-Molecules with Inorganic Molecular-Species into Nanocomposite Biphase Arrays. *Chem. Mater.* **1994**, *6*, 1176-1191.
18. Huo, Q. S.; Margolese, D. I.; Ciesla, U.; Feng, P. Y.; Gier, T. E.; Sieger, P.; Leon, R.; Petroff, P. M.; Schuth, F.; Stucky, G. D., Generalized Synthesis of Periodic Surfactant Inorganic Composite-Materials. *Nature* **1994**, *368*, 317-321.
19. Huo, Q. S.; Leon, R.; Petroff, P. M.; Stucky, G. D., Mesostructure Design with Gemini Surfactants - Supercage Formation in a 3-Dimensional Hexagonal Array. *Science* **1995**, *268*, 1324-1327.
20. Huo, Q. S.; Margolese, D. I.; Stucky, G. D., Surfactant Control of Phases in the Synthesis of Mesoporous Silica-Based Materials. *Chem. Mater.* **1996**, *8*, 1147-1160.
21. Zhao, D. Y.; Feng, J. L.; Huo, Q. S.; Melosh, N.; Fredrickson, G. H.; Chmelka, B. F.; Stucky, G. D., Triblock Copolymer Syntheses of Mesoporous Silica with Periodic 50 to 300 Angstrom Pores. *Science* **1998**, *279*, 548-552.
22. Zhao, D. Y.; Huo, Q. S.; Feng, J. L.; Chmelka, B. F.; Stucky, G. D., Nonionic Triblock and Star Diblock Copolymer and Oligomeric Surfactant Syntheses of Highly Ordered, Hydrothermally Stable, Mesoporous Silica Structures. *J. Am. Chem. Soc.* **1998**, *120*, 6024-6036.
23. Han, L.; Che, S., Anionic Surfactant Templated Mesoporous Silicas (Amss). *Chem. Soc. Rev.* **2013**, *42*, 3740-3752.
24. Soler-illia, G. J. D.; Sanchez, C.; Lebeau, B.; Patarin, J., Chemical Strategies to Design Textured Materials: From Microporous and Mesoporous Oxides to Nanonetworks and Hierarchical Structures. *Chem. Rev.* **2002**, *102*, 4093-4138.
25. Hench, L. L.; West, J. K., The Sol-Gel Process. *Chem. Rev.* **1990**, *90*, 33-72.
26. Bruinsma, P. J.; Kim, A. Y.; Liu, J.; Baskaran, S., Mesoporous Silica Synthesized by Solvent Evaporation: Spun Fibers and Spray-Dried Hollow Spheres. *Chem. Mater.* **1997**, *9*, 2507-2512.
27. Israelachvili, J. N., *Intermolecular and Surface Forces*, 3 ed.; Elsevier: USA, 2011.
28. B. Jönsson, B. L., K. Holmberg, B. Kronberg, *Surfactants and Polymers in Aqueous Solution*; John Wiley & sons, 1998, p 61-89.
29. Balmbra, R. R.; Clunie, J. S.; Goodman, J. F., Cubic Mesomorphic Phases. *Nature* **1969**, *222*, 1159-&.
30. Brinker, C. J., Hydrolysis and Condensation of Silicates - Effects on Structure. *J. Non-Cryst. Solids* **1988**, *100*, 31-50.
31. Iler, P. K., *The Chemistry of Silica*; John Wiley & Sons: Canada, 1979, p 135-137.
32. Kajihara, K., Recent Advances in Sol–Gel Synthesis of Monolithic Silica and Silica-Based Glasses. *J. Asian Ceram. Soc.* **2013**, 13.

33. Hahn, T., *Interational Tables for Crystallography-Volume A: Space-Group Symmetry*. 5 ed.; Kluwer Academic Publishers: Dordrecht, Boston and London, 2002; Vol. A.
34. Svensson, A.; Piculell, L.; Karlsson, L.; Cabane, B.; Jonsson, B., Phase Behavior of an Ionic Surfactant with Mixed Monovalent/Polymeric Counterions. *J. Phys. Chem. B* **2003**, *107*, 8119-8130.
35. Kaneko, D.; Olsson, U.; Sakamoto, K., Self-Assembly in Some N-Lauroyl-L-Glutamate/Water Systems. *Langmuir* **2002**, *18*, 4699-4703.
36. Fontell, K., Cubic Phases in Surfactant and Surfactant-Like Lipid Systems. *Colloid. Polym. Sci.* **1990**, *268*, 264-285.
37. Soni, S. S.; Brotons, G.; Bellour, M.; Narayanan, T.; Gibaud, A., Quantitative Saxs Analysis of the P123/Water/Ethanol Ternary Phase Diagram. *J. Phys. Chem. B* **2006**, *110*, 15157-15165.
38. Liu, C. K.; Warr, G. G., Hexagonal Closest-Packed Spheres Liquid Crystalline Phases Stabilised by Strongly Hydrated Counterions. *Soft Matter* **2014**, *10*, 83-87.
39. Delacroix, H.; Gulikkrzywicki, T.; Mariani, P.; Luzzati, V., Freeze-Fracture Electron-Microscope Study of Lipid Systems - the Cubic Phase of Space Group Pm3n. *J. Mol. Biol.* **1993**, *229*, 526-539.
40. Soderman, O.; Walderhaug, H.; Henriksson, U.; Stilbs, P., Nmr Relaxation in Isotropic Surfactant Systems - a H-2, C-13, and N-14 Nmr-Study of the Micellar (L1) and Cubic (I1) Phases in the Dodecyltrimethylammonium Chloride Water-System. *J. Phys. Chem.* **1985**, *89*, 3693-3701.
41. Eriksson, P. O.; Lindblom, G.; Arvidson, G., Nmr-Studies of Micellar Aggregates in 1-Acyl-Sn-Glycerophosphocholine Systems - the Formation of a Cubic Liquid-Crystalline Phase. *J. Phys. Chem.* **1987**, *91*, 846-853.
42. Imai, M.; Yoshida, I.; Iwaki, T.; Nakaya, K., Static and Dynamic Structures of Spherical Nonionic Surfactant Micelles During the Disorder-Order Transition. *J. Chem. Phys.* **2005**, *122*.
43. Sakamoto, Y.; Han, L.; Che, S.; Terasaki, O., Structural Analyses of Intergrowth and Stacking Fault in Cage-Type Mesoporous Crystals. *Chemistry of Materials* **2009**, *21*, 223-229.
44. Delacroix, H.; GulikKrzywicki, T.; Seddon, J. M., Freeze Fracture Electron Microscopy of Lyotropic Lipid Systems: Quantitative Analysis of the Inverse Micellar Cubic Phase of Space Group Fd3m (Q(227)). *J. Mol. Biol.* **1996**, *258*, 88-103.
45. Seddon, J. M.; Robins, J.; Gulik-Krzywicki, T.; Delacroix, H., Inverse Micellar Phases of Phospholipids and Glycolipids. *PCCP* **2000**, *2*, 4485-4493.
46. Ma, Y. H.; Han, L.; Miyasaka, K.; Oleynikov, P.; Che, S. N.; Terasaki, O., Structural Study of Hexagonal Close-Packed Silica Mesoporous Crystal. *Chem. Mater.* **2013**, *25*, 2184-2191.
47. Besson, S.; Gacoin, T.; Ricolleau, C.; Jacquiod, C.; Boilot, J. P., Phase Diagram for Mesoporous Ctab-Silica Films Prepared under Dynamic Conditions. *J. Mater. Chem.* **2003**, *13*, 404-409.
48. Sakamoto, Y.; Diaz, I.; Terasaki, O.; Zhao, D. Y.; Perez-Pariente, J.; Kim, J. M.; Stucky, G. D., Three-Dimensional Cubic Mesoporous Structures of Sba-12 and Related Materials by Electron Crystallography. *J. Phys. Chem. B* **2002**, *106*, 3118-3123.
49. Clerc, M., A New Symmetry for the Packing of Amphiphilic Direct Micelles. *J. Phys. II* **1996**, *6*, 961-968.

50. Zeng, X. B.; Liu, Y. S.; Imperor-Clerc, M., Hexagonal Close Packing of Nonionic Surfactant Micelles in Water. *J. Phys. Chem. B* **2007**, *111*, 5174-5179.
51. Klein, R.; Tiddy, G. J. T.; Maurer, E.; Touraud, D.; Esquena, J.; Tache, O.; Kunz, W., Aqueous Phase Behaviour of Choline Carboxylate Surfactants-Exceptional Variety and Extent of Cubic Phases. *Soft Matter* **2011**, *7*, 6973-6983.
52. Shearman, G. C.; Tyler, A. I. I.; Brooks, N. J.; Templer, R. H.; Ces, O.; Law, R. V.; Seddon, J. M., A 3-D Hexagonal Inverse Micellar Lyotropic Phase. *J. Am. Chem. Soc.* **2009**, *131*, 1678-+.
53. Gustavsson, C.; Li, J. Q.; Edler, K. J.; Piculell, L., Water-Responsive Internally Structured Polymer Surfactant Films on Solid Surfaces. *Langmuir* **2014**, *30*, 12525-12531.
54. Gustavsson, C.; Obiols-Rabasa, M.; Piculell, L., Water-Insoluble Surface Coatings of Polyion-Surfactant Ion Complex Salts Respond to Additives in a Surrounding Aqueous Solution. *Langmuir* **2015**, *31*, 6487-6496.
55. Sakya, P.; Seddon, J. M.; Templer, R. H.; Mirkin, R. J.; Tiddy, G. J. T., Micellar Cubic Phases and Their Structural Relationships: The Nonionic Surfactant System C12eo12/Water. *Langmuir* **1997**, *13*, 3706-3714.
56. Mau, S. C.; Huse, D. A., Stacking Entropy of Hard-Sphere Crystals. *Physical Review E* **1999**, *59*, 4396-4401.
57. Zhao, D. Y.; Huo, Q. S.; Feng, J. L.; Kim, J. M.; Han, Y. J.; Stucky, G. D., Novel Mesoporous Silicates with Two-Dimensional Mesostructure Direction Using Rigid Bolaform Surfactants. *Chem. Mater.* **1999**, *11*, 2668-2672.
58. Jin, C. Y.; Han, L.; Che, S. A., Synthesis of a DNA-Silica Complex with Raire Two-Dimensional Square P4mm Symmetry. *Angewandte Chemie-International Edition* **2009**, *48*, 9268-9272.
59. Gao, C.; Che, S., Organically Functionalized Mesoporous Silica by Co-Structure-Directing Route. *Adv. Funct. Mater.* **2010**, *20*, 2750-2768.
60. Che, S.; Garcia-Bennett, A. E.; Yokoi, T.; Sakamoto, K.; Kunieda, H.; Terasaki, O.; Tatsumi, T., A Novel Anionic Surfactant Templating Route for Synthesizing Mesoporous Silica with Unique Structure. *Nature Materials* **2003**, *2*, 801-805.
61. Zheng, H. Q.; Gao, C. B.; Che, S. N., Amino and Quaternary Ammonium Group Functionalized Mesoporous Silica: An Efficient Ion-Exchange Method to Remove Anionic Surfactant from Ams. *Microporous and Mesoporous Materials* **2008**, *116*, 299-307.
62. Qiu, H. B.; Che, S. N., Chiral Mesoporous Silica: Chiral Construction and Imprinting Via Cooperative Self-Assembly of Amphiphiles and Silica Precursors. *Chem. Soc. Rev.* **2011**, *40*, 1259-1268.
63. Garcia-Bennett, A. E.; Terasaki, O.; Che, S.; Tatsumi, T., Structural Investigations of Ams-N Mesoporous Materials by Transmission Electron Microscopy. *Chem. Mater.* **2004**, *16*, 813-821.
64. Garcia-Bennett, A. E.; Kupferschmidt, N.; Sakamoto, Y.; Che, S.; Terasaki, O., Synthesis of Mesocage Structures by Kinetic Control of Self-Assembly in Anionic Surfactants. *Angewandte Chemie-International Edition* **2005**, *44*, 5317-5322.
65. Gao, C. B.; Sakamoto, Y.; Sakamoto, K.; Terasaki, O.; Che, S. N., Synthesis and Characterization of Mesoporous Silica Ams-10 with Bicontinuous Cubic Pn3m Symmetry. *Angewandte Chemie-International Edition* **2006**, *45*, 4295-4298.

66. Gao, C. B.; Sakamoto, Y.; Terasaki, O.; Che, S. A., Formation of Diverse Mesophases Templated by a Diprotic Anionic Surfactant. *Chemistry-a European Journal* **2008**, *14*, 11423-11428.

67. Gao, C.; Sakamoto, Y.; Terasaki, O.; Sakamoto, K.; Che, S., Molecular Design of the Surfactant and the Co-Structure-Directing Agent (Csda) toward Rational Synthesis of Targeted Anionic Surfactant Templated Mesoporous Silica. *J. Mater. Chem.* **2007**, *17*, 3591-3602.

68. Han, L.; Sakamoto, Y.; Terasaki, O.; Li, Y.; Che, S., Synthesis of Carboxylic Group Functionalized Mesoporous Silicas (Cfmss) with Various Structures. *J. Mater. Chem.* **2007**, *17*, 1216-1221.

69. Han, L.; Sakamoto, Y.; Che, S.; Terasaki, O., Insight into the Defects of Cage-Type Silica Mesoporous Crystals with *Fd*-3*m* Symmetry: Tem Observations and a New Proposal of "Polyhedron Packing" for the Crystals. *Chem. Eur. J.* **2009**, *15*, 2818-2825.

70. Han, L. Synthesis and Characterization of Functionalized Silica Mesoporous Crystals. Stockholm University, Stockholm, Sweden, 2010.

71. Che, S.; Liu, Z.; Ohsuna, T.; Sakamoto, K.; Terasaki, O.; Tatsumi, T., Synthesis and Characterization of Chiral Mesoporous Silica. *Nature* **2004**, *429*, 281-284.

72. Nnanna, I. A.; Xia, J., *Protein-Based Surfactants - Synthesis, Physicochemical Properties, and Applications*. Marcel Dekker, Inc.: USA, 2001; Vol. 101.

73. Jin, H. Y.; Liu, Z.; Ohsuna, T.; Terasaki, O.; Inoue, Y.; Sakamoto, K.; Nakanishi, T.; Ariga, K.; Che, S. N., Control of Morphology and Helicity of Chiral Mesoporous Silica. *Adv. Mater.* **2006**, *18*, 593-+.

74. Jin, H. Y.; Qiu, H. B.; Sakamoto, Y.; Shu, P.; Terasaki, O.; Che, S. N., Mesoporous Silicas by Self-Assembly of Lipid Molecules: Ribbon, Hollow Sphere, and Chiral Materials. *Chemistry-a European Journal* **2008**, *14*, 6413-6420.

75. Goldstein, J. I.; Newbury, D. E.; Echlin, P.; Joy, D. C.; A. D. Romig, J.; Lyman, C. E.; Fiori, C.; Lifshin, E., *Scanning Electron Microscopy and X-Ray Microanalysis - a Text for Biologists, Materials Scientists, and Geologists* Plenum Press, New York, 1992.

76. Sing, K. S. W.; Everett, D. H.; Haul, R. A. W.; Moscou, L.; Pierotti, R. A.; Rouquerol, J.; Siemieniewska, T., Reporting Physisorption Data for Gas Solid Systems with Special Reference to the Determination of Surface-Area and Porosity (Recommendations 1984). *Pure Appl. Chem.* **1985**, *57*, 603-619.

77. Williams, D. B.; Carter, C. B., *Transmission Electron Microscopy - a Textbook for Materials Science*; Springer US, 1996.

78. Glatter, O., New Method for Evaluation of Small-Angle Scattering Data. *J. Appl. Crystallogr.* **1977**, *10*, 415-421.

79. Sasview for Small Angle Scattering Analysis: A Sas Community Project Launched from the Nsf Danse Effort; http://www.sasview.org/.

80. Guinier, A.; Fournet, G., *Small-Angle Scattering of X-Rays*; John Wiley and Sons: New York, 1955.

81. Hayter, J. B.; Penfold, J., An Analytic Structure Factor for Macroion Solutions. *Mol. Phys.* **1981**, *42*, 109-118.

82. Hansen, J. P.; Hayter, J. B., A Rescaled Msa Structure Factor for Dilute Charged Colloidal Dispersions. *Mol. Phys.* **1982**, *46*, 651-656.

83. Smart, L. E.; Moore, E. A., *Solid State Chemistry: An Introduction*; CRC Press, Taylar & Francis Group, 2005.

84. Petricek, V.; Dusek, M.; Palatinus, L., Crystallographic Computing System Jana2006: General Features. *Zeitschrift Fur Kristallographie* **2014**, *229*, 345-352.

85. The Stoe Powder Diffraction Software Package Winxpow
https://www.stoe.com/product/software-powder-xrd/.

86. Toby, B. H.; Von Dreele, R. B., Gsas-Ii: The Genesis of a Modern Open-Source All Purpose Crystallography Software Package. *J. Appl. Crystallogr.* **2013**, *46*, 544-549.

87. Cui, H.; Hodgdon, T. K.; Kaler, E. W.; Abezgauz, L.; Danino, D.; Lubovsky, M.; Talmon, Y.; Pochan, D. J., Elucidating the Assembled Structure of Amphiphiles in Solution Via Cryogenic Transmission Electron Microscopy. *Soft Matter* **2007**, *3*, 945-955.

88. Milne, J. L. S.; Borgnia, M. J.; Bartesaghi, A.; Tran, E. E. H.; Earl, L. A.; Schauder, D. M.; Lengyel, J.; Pierson, J.; Patwardhan, A.; Subramaniam, S., Cryo-Electron Microscopy - a Primer for the Non-Microscopist. *Febs Journal* **2013**, *280*, 28-45.

89. Bellare, J. R.; Davis, H. T.; Scriven, L. E.; Talmon, Y., Controlled Environment Vitrification System - an Improved Sample Preparation Technique. *Journal of Electron Microscopy Technique* **1988**, *10*, 87-111.

90. Falls, A. H.; Wellinghoff, S. T.; Talmon, Y.; Thomas, E. L., A Transmission Electron-Microscopy Study of Hexagonal Ice. *Journal of Materials Science* **1983**, *18*, 2752-2764.

91. Harris, R. K., *Nuclear Magnetic Resonance Spectroscopy - a Physicochemical View*; Longman Scientific & Technical, John Wiley & Sons, Inc.: Harlow, UK, and New York, USA, 1994.

92. Nowacka, A.; Mohr, P. C.; Norrman, J.; Martin, R. W.; Topgaard, D., Polarization Transfer Solid-State Nmr for Studying Surfactant Phase Behavior. *Langmuir* **2010**, *26*, 16848-16856.

93. Nowacka, A.; Bongartz, N. A.; Ollila, O. H. S.; Nylander, T.; Topgaard, D., Signal Intensities in H-1-C-13 Cp and Inept Mas Nmr of Liquid Crystals. *J. Magn. Reson.* **2013**, *230*, 165-175.

94. Nowacka, A.; Douezan, S.; Wadso, L.; Topgaard, D.; Sparr, E., Small Polar Molecules Like Glycerol and Urea Can Preserve the Fluidity of Lipid Bilayers under Dry Conditions. *Soft Matter* **2012**, *8*, 1482-1491.

95. Pines, A.; Waugh, J. S.; Gibby, M. G., Proton-Enhanced Nuclear Induction Spectroscopy - Method for High-Resolution Nmr of Dilute Spins in Solids. *J. Chem. Phys.* **1972**, *56*, 1776

96. Morris, G. A.; Freeman, R., Enhancement of Nuclear Magnetic-Resonance Signals by Polarization Transfer. *J. Am. Chem. Soc.* **1979**, *101*, 760-762.

97. Alonso, B.; Massiot, D., Mufti-Scale Nmr Characterisation of Mesostructured Materials Using H-1 -> C-13 through-Bond Polarisation Transfer, Fast Mas, and H-1 Spin Diffusion. *J. Magn. Reson.* **2003**, *163*, 347-352.

98. Elena, B.; Lesage, A.; Steuernagel, S.; Bockmann, A.; Emsley, L., Proton to Carbon-13 Inept in Solid-State Nmr Spectroscopy. *J. Am. Chem. Soc.* **2005**, *127*, 17296-17302.

99. Warschawski, D. E.; Devaux, P. F., H-1-C-13 Polarization Transfer in Membranes: A Tool for Probing Lipid Dynamics and the Effect of Cholesterol. *J. Magn. Reson.* **2005**, *177*, 166-171.

100. Steel, A.; Carr, S. W.; Anderson, M. W., Si-29 Solid-State Nmr-Study of Mesoporous M41s Materials. *Chem. Mater.* **1995**, *7*, 1829-1832.

101. Sugahara, Y.; Inoue, T.; Kuroda, K., Si-29 Nmr Study on Co-Hydrolysis Processes in Si(Oet)(4)-Rsi(Oet)(3)-Etoh-Water-Hcl Systems (R=Me,Ph): Effect of R Groups. *J. Mater. Chem.* **1997**, *7*, 53-59.

102. Acd/Nmr Processor Academic Edition; http://www.acdlabs.com/resources/freeware/nmr_proc/.

103. Evilevitch, A.; Lobaskin, V.; Olsson, U.; Linse, P.; Schurtenberger, P., Structure and Transport Properties of a Charged Spherical Microemulsion System. *Langmuir* **2001**, *17*, 1043-1053.

104. Armon, S.; Efrati, E.; Kupferman, R.; Sharon, E., Geometry and Mechanics in the Opening of Chiral Seed Pods. *Science* **2011**, *333*, 1726-1730.

105. Forterre, Y.; Dumais, J., Generating Helices in Nature. *Science* **2011**, *333*, 1715-1716.

I was born in 1988. Until I was 5 years old I lived in a small city called Altay which at that time had, according to my father, less than 170 thousand inhabitants. At age 5 I moved with my parents to Urumqi, the capital city of Xinjiang province (Autonomous Region), 700 km, 7 hours driving, from Altay, which then became my home. Since I can recall, I spent my whole childhood in Urumqi, and the education before University.

After 3 years of high school where my studies were focused on Nature Science, in 2006, I went to Shanghai, to do a degree in Chemistry at Shanghai Jiao Tong University. Nowadays Shanghai has about 25 million inhabitants and is 3200 km, 5 hours flight, from Urumqi. In 2010, I completed my university studies and decided to come to Lund as a guest student for 3 month.

The Swedish working environment in Lund immediately attracted me, and I made one big decision, to continue my study and do a PhD in Lund. Lund has 117 thousand inhabitants and about 8000 km from Shanghai however 5000 km from Urumqi, so some how not much further than Shanghai. After a 6 years stay, that was a wise decision, it led to this!

Jessie

Printed by Media-Tryck, Lund University 2016
Nordic Ecolabel 3041 0903

LUND UNIVERSITY

ISBN 978-91-7422-483-2

Physical Chemistry
Department of Chemistry
Faculty of Science
Lund University